PROJECT COMPLETION REPORT

FOR THE PERIOD 09-12-2015 TO 08-12-2020

EXTENSION UP TO 09-06-2021

PROGRAMME :

"**Programme Support on Translational Research on Biomaterials for Orthopaedic and Dental applications"**

PROJECT TITLE :

PROJECT III in the Programme:

Design of dental implant using Titanium-Hydroxyapatite Composites and Hydroxyapatite-based Dual Ceramic Coating on Dental Implant System

INVESTIGATORS TEAM :

Prof. Bikramjit Basu, Professor, Materials Research Center, Indian Institute of Science (IISc), Bangalore – 560012

Dr. H. K. Varma, Scientist, Biomedical Technology Wing, SCTIMST, Thiruvananthapuram

Dr. Manoj Komath, Scientist, Biomedical Technology Wing, SCTIMST, Thiruvananthapuram

Dr. A. Sabareeswaran, Biomedical Technology Wing, SCTIMST, Thiruvananthapuram

PROJECT REPORT PART B - WORK DONE at SCTIMST

1. INTRODUCTION

1.1 Dental Implants

Dental implant system is becoming more and more popular in the present day dental surgery. In the past 20 years, the number of dental implant procedures has increased steadily worldwide, reaching about one million dental implantations per year. [Le Gu´ehennec L., Soueidan A., Layrolle P., Amouriq Y., Surface treatments of titanium dental implants for rapid osseointegration, Dental Materials 23 (2007) 844-854]. A typical dental implant system consists of metallic tooth root and attachment components made of metal (preferably titanium alloy) to support a dental prosthesis. This helps to make a semi-permanent fitting of crown, bridge and denture, by making them implant-supported that resembles natural teeth. The implant prosthesis systems available now in the International market give more predictable outcome and better reliable treatment option than traditional restorations.

The current implant-making technology offers a matured and reliable system, offering long term success after implantation. The system consists of an 'implant' part which goes into the bone and provide a stable anchorage, and an 'abutment' part which connects the prosthetic crown to the implant. This multi-component structure is designed for the convenience of surgery and tooth prosthesis placement. The size, shape and form of the components will vary according to the position of the implant.

1.2 Biological Stability of a Dental Implant

The clinical success of the implantation is mainly decided by the 'stability' parameter, which in turn is related to their early osseointegration [Le Gu´ehennec L., Soueidan A., Layrolle P., Amouriq Y., Surface treatments of titanium dental implants for rapid osseointegration, Dental Materials 23 (2007) 844-854]. Geometry and surface topography are crucial for the short-term and long-term success of dental implants. These parameters are linked with delicate surgical techniques, a pre-requisite for a successful early clinical outcome.

Titanium implant screw, up on implantation, interacts with biological fluids and tissues. Direct bone apposition onto the surface of the titanium is critical for the rapid loading of the screw. After the initial stages of osseointegration, both prosthetic biomechanical factors and patient hygiene are crucial for the long-term success of the implants. There are two types of response after implantation. The first type involves the formation of a fibrous soft tissue capsule around the implant. This fibrous tissue capsule does not ensure proper biomechanical fixation and leads to clinical failure of the dental implant. The second type of bone response is related to direct bone-to-implant contact without an intervening connective tissue layer. This biological fixation is called 'osseointegration'. It is considered to be a pre-requisite for the long-term success of implant prostheses. The rate and quality of osseointegration in titanium implants are related to their surface properties. Surface composition, hydrophilicity and roughness are main parameters that influence the implant–tissue interaction and osseointegration.

1.3 Modification of implant surface :

The knowledge about the interaction of materials and tissues indicate that an appropriate modification of the titanium surface will enhance the osseointegration. One accepted method is to coat the surface with layers of calcium phosphate minerals, mainly hydroxyapatite (the bone mineral). Following implantation, the release of calcium phosphate into the peri-implant region increases the saturation of body fluids and precipitates a biological apatite onto the surface of the implant. This layer of biological apatite contains endogenous proteins and serves as a matrix for osteogenic cell attachment and growth. The bone healing process around the implant is therefore enhanced by this biological apatite layer.

It is well-recognized that calcium phosphate coatings have led to better clinical success rates in the long-term than uncoated titanium implants. Different methods have been developed to coat metal implants, like plasma spraying, sputter-deposition, sol-gel coating, electrophoretic deposition and biomimetic precipitation. Out of these, only the plasma-spraying coating method has been proven to be commercially viable. Currently, top rated implants are sold with plasma spray coated hydroxyapatite layer.

Plasma-spraying is a technique in which hydroxyapatite (HA) ceramic particles are injected into a plasma torch burning at high temperature and projected on to the surface of the titanium where the particles condense and fuse together, forming a coating. The process allows only high coating thickness, with a minimum of few hundred micrometers. In order to obtain mechanical retention of the coating, the surface of the metallic implant must be roughened by means of grit blasting. The problems found in coatings are porosity, residual stress at the substrate/coating interface, as well as drastic changes in the composition and crystallinity of the initial layers. Moreover, the plasma-spraying technique is not very effective for coating tiny dental implants with a complex shape.

One of the major concerns with plasma-sprayed coatings in clinical use is the possible delamination of the coating from the surface of the titanium implant. This usually happens when the implants are inserted into dense bone. The delamination will lead to particle release to the tissues and to the eventual failure of implants. Therefore, the surgeons are skeptical about the use of coated titanium screws for implantation. However, in the meta-analyses of clinical trials, the long-term survival rates of plasma-sprayed HA-coated dental implants were not inferior compared to uncoated dental implants.

1.4 Need for modifying the abutment structure:

Another challenge faced by the implant system is the stability of the joint of abutment. This is a function of the geometry of the implant, the contact between the implant head and the abutment screw bore, the material construction of the implant and the friction between the various implant parts [Balfour A, O'Brien GR. Comparative study of anti-rotational single tooth abutments. Prosthet Dent. 73 (1995) 36–43]. Abutment loosening is a problem which is mainly caused by the friction, particularly at the top of the implants. Materials with special characteristics, in particular those that are lightweight, strong, durable and resistant to wear, are very useful as anti-frictional agents. The use of such protective coatings is not reported yet on abutments.

1.5 Background of the work

Any failure in osteointegration of the implant and abutment loosening, can drastically reduce the useful life of the implant. It has been suggested that adherent hydroxyapatite coating of submicron thickness (~ 400nm) will be more effective. Coating technologies alternative to plasma spray are being explored to achieve this. The abutment joint could be protected by applying hard and low-friction coatings.

The investigators' team in SCTIMST has developed coatings technology to solve the issues currently observed in an implant system. They have developed indigenous processes for coating hydroxyapatite (HA) and diamond-like carbon (DLC) on titanium metal. Hydroxyapatite is coated through Pulsed Laser Deposition (PLD) technique, which can provide sub-micron thick conformal hydroxyapatite coating. This will be an alternative to thick plasma sprayed coating on the implant part, which can give better clinical outcomes. The friction of the abutment joint could be drastically reduced by DLC coating. This process is based on Plasma Enhanced Chemical Vapour Deposition (PECVD) technique. The project work was planned in this background.

Several companies are making the implant system and marketing globally. About 106 manufacturers are notified by International Congress of Oral Implantologists, Wayne, New Jersey (http://icoi.org/implant-manufacturers-list.php). Many of these manufacturers are providing hydroxyapatite coated (plasma spray) implants. In the recent years, more and more patients prefer single tooth prosthesis and the need for dental implant is increasing. Almost all of the Indian suppliers import and distribute the implant systems. Despite the need among the population, very limited research had occurred on implant system in India. Some systems were made indigenously by researchers at Defense Research and Development Organisation (DRDO) in 2004 and by a team in Delhi IIT a decade later. Therefore, the research on improved implant systems has relevance in biomedical technology.

In the project, we envisaged a dual-coated implant system which is schematically represented in Figure 1.

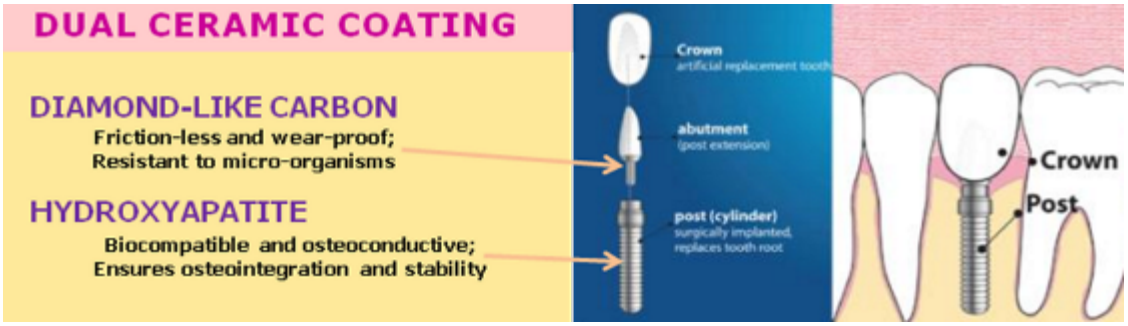

Figure 1. Schematic of a dual-coated dental implant system

The work planned was the indigenous design of the implant system, coating the implant surface with hydroxyapatite (500nm layer) in the semi-industrial pulsed laser coating system, coating the abutment surface with adherent Diamond-like Carbon using the PECVD coating system, testing the coated system for biocompatibility as per ISO 10993 and testing the efficacy of the coating by implanting in an animal model.

1.6 Objectives

The work has been planned with the following objectives

1. To design appropriate CAD based model for tooth replacement and to evaluate the design parameters using finite element analysis to match patient specificity.
2. To fabricate the implant using 3D printing technology and to assess the cyto-compatibility properties in vitro.
3. To develop a prototype of ceramic coated dental implants using state-of-art coating deposition techniques.
4. To carry out the pre-clinical tests in appropriate animal models involving histopathologist.
5. To study the local effects of surface modified dental materials using histological analysis.
6. To study the cellular and molecular effects of dental implants developed in this collaborative research proposal via detailed bone marker analysis using RT-PCR.
7. To study the product validation, assessment of Technology Readiness Level (TRL) and to explore the possibility of technology transfer to biomedical companies involving an entrepreneur.

The work flow between the collaborators – a graphical chart

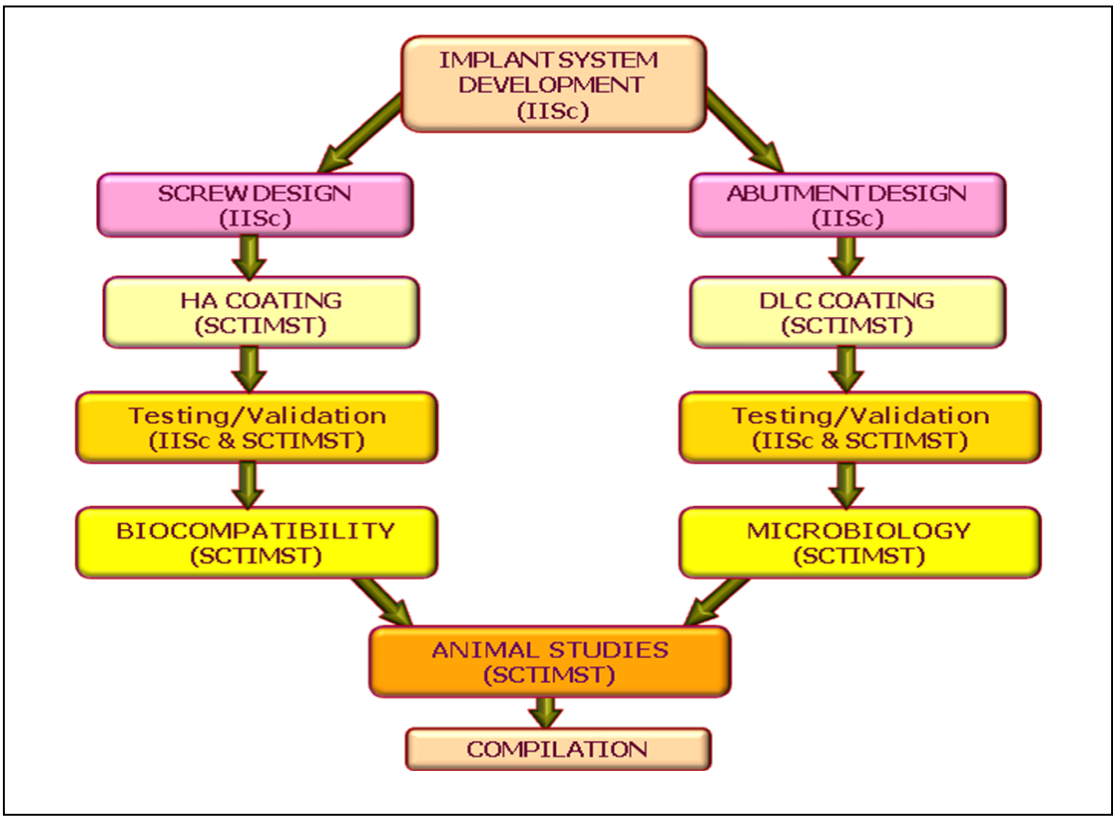

2. DEVELOPMENT OF DIAMOND-LIKE CARBON (DLC) COATING

2.1 Fundamentals about the DLC materials

The class of Diamond-like Carbons signifies a range of compositions of carbon got synthesized along with the advancement of materials science. The thin film deposition technology enabled the formation of amorphous carbon structures at thermodynamically metastable conditions, with varying sp^2 and sp^3 bonds. The usage of hydrocarbon precursors for the synthesis led to the inclusion of hydrogen, which terminate the sites of double bonding of carbon. The carbon films obtained thus showed a unique combination of properties, the ranges of which could be tuned.

According to the carbon species ratio (sp^2 to sp^3) and the amount of hydrogen, these films are classified as - tetrahedral amorphous carbon (ta-C), hydrogenated amorphous carbon (a-C:H), and amorphous carbon without hydrogen (a-C). Compared to other thin film materials, they have a combination of superior properties, including remarkable chemical inertness, low coefficient of friction, high resistance to wear, high thermal conductivity, high electrical resistivity and excellent biocompatibility. For the same reason, they found numerous novel applications, over the past 4 decades or so. Currently, it is accepted that the term 'Diamond-like Carbon' (DLC) refers to amorphous hydrogenated carbon (a-C:H).

DLC can be deposited by several methods, including chemical vapour deposition, cathodic arc deposition, pulsed laser deposition, direct ion beam deposition, ion beam conversion of condensed precursor, magnetron sputtering, plasma source ion deposition and direct current/radiofrequency sputtering. The techniques and the precursors used in the coating process dictate the composition and structure, and thereby the properties. DLC films have a wide range of applications, such as in electric and electronic equipment, in cutting tools, molds and automotive parts, in optical components and in various household items.

DLC coating provides excellent haemocompatibility and biocompatibility along with low wear and good stability in physiological conditions, which makes it useful for crucial biomedical applications, especially in orthopedic and cardiovascular devices.

One sub-objective of the project is the development of DLC coating on the abutment. Process development was done and the coating was subjected to various tests and analyses, the details of which are given in the following sections.

2.2 Process development for DLC Coating

The process development of DLC coatings was done in the plasma enhanced chemical vapour deposition (PECVD) system, available in the lab of the Investigators. The system consists of a stainless steel high vacuum chamber with radiofrequency (RF) power for inducing plasma at low pressures in the contained gas/vapour. The desired gas or

vapour, alone or in combination at required flow rate could be drawn to the chamber using a gas/vapour flow manifold. The chamber could be pumped down to high vacuum (10^{-6} mbar) and then brought to working pressure (10^{-2} mbar) using a servo-controlled butterfly valve. The system is fully automated and interfaced with computer, so that the process steps (with parameters of step duration, RF power, individual vapour/gas flow rates and pressure) could be programmed and executed.

The coatings were done on Titanium metal (ASTM F Grade used for dental implants) and 3D printed Titanium composite). High care is taken for sample preparation, as the surface micromorphology and cleanliness play crucial roles in improving the adhesion of the coating. Metal coupons were polished manually and mechanically to a level of 0.02 microns R_a value (However, this polish was not achievable in printed Titanium composite samples because of the inherent porous nature). The samples were cleaned by ultrasonication in soap solution and distilled water and dried in a hot air oven.

The samples were loaded in the chamber and *in situ* sputter cleaning was done initially in high pure hydrogen and argon, to get rid of remnant impurities or oxides. In the coating process, a silicon-based inter-layer was deposited at first, by admitting the vapours of tetra methyl silane. The role of this inter-layer is to enhance the adhesion of the diamond-like carbon coating onto the metal. The diamond-like carbon (DLC) layer was deposited seamlessly over the previous layer in a continuing process step, using cyclohexane. The flow rate, bias potential and process pressures were in the range, 12-20 sccm, 350V-500V and $1X10^{-2}$ - $5X10^{-2}$ mbar respectively.

Process optimization was done based on acceptance criteria for the coating which can meet the requirements of the intended application. The important criterion is related to the deposition rate. The rate should be in the range of 1 micron in a period of 1 hour, to make the process commercially viable. Process repeatability should be within 5% (for a minimum of 16 measurements). Coating uniformity should be in an acceptable range, not less than 10% variation across 30cm high and 30cm diameter volume above the electrode.

2.3 DLC Coating Characterization

Coatings were made with the above process parameters and subjected to characterization to understand the various features/ properties. The most important ones are - the chemical composition, the carbon species present, surface roughness, microhardness, modulus and adhesion strength. The tests and characterization were done on 1 micron thick coating on AISI316 stainless steel.

The coatings produced were found amorphous in X-ray diffractometry. No long range order or crystalline inclusions were found. In FTIR analysis, the individual layers were prepared on thin KBr pellets in a thickness 500nm and analysed. The aim was to identifying the chemical nature of the inter-layer and the carbon layer.

The FTIR spectrum of the DLC layer (deposited using cyclohexane) given in figure 2 shows peaks corresponding to C-CH_3 and C=C (sp^2). The presence of C-H bonds is evident , with peaks of CH_3 (sp^2 & sp^3) and CH_2 (sp^3). The material could be understood to be “Amorphous Hydrogenated Diamond-Like Carbon (a-C:H)”

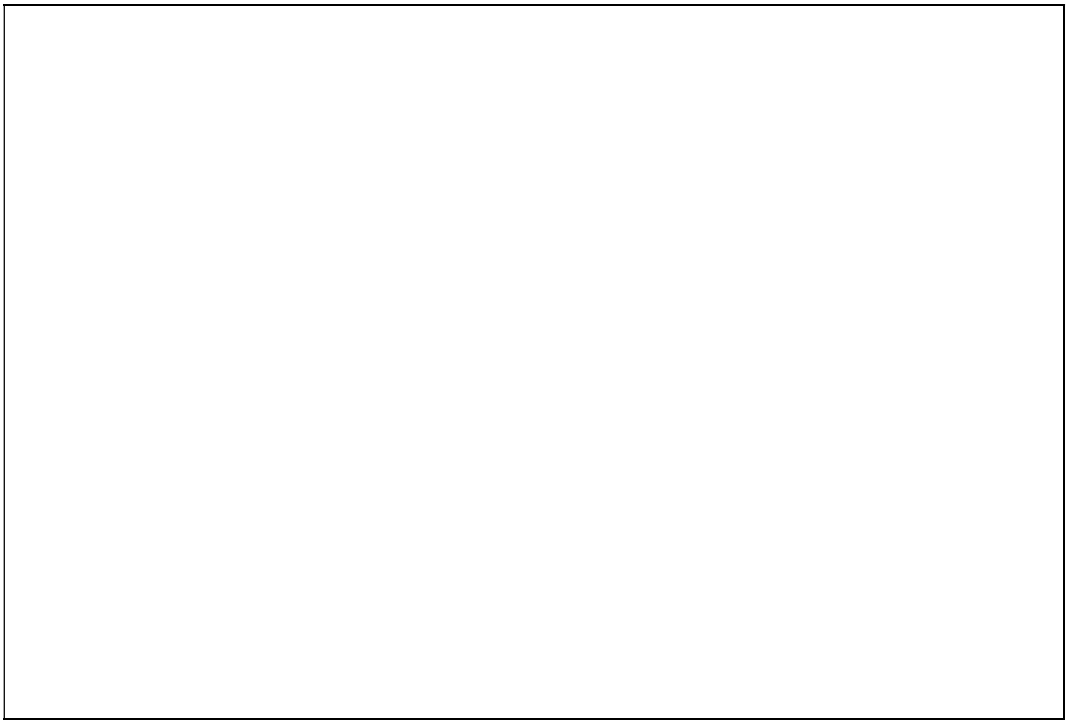

Figure 2. FTIR of the DLC layer deposited on KBr window

The coating has been subjected to Raman analysis in WITec alpha 300R Confocal Raman system with 532 nm NdYAG laser. The Raman spectrum of the coating is given in Figure 3. There are two prominent, but broad, peaks in the spectrum of the coating, at 1585 cm^{-1} and at 1354 cm^{-1}. These are typical with amorphous diamond-like carbon films [Ref: Ferrari AC, Determination of bonding in diamond-like carbon by Raman spectroscopy, Diamond and Related Materials 11 (2002) 1053; Schwan J, Ulrich S, Batori V, and Ehrhardt H, and Silva SRP, Raman spectroscopy on amorphous carbon films, J. Appl. Phys. 80 (1996) 440].

Raman spectrum of amorphous carbon gives information about sp^2 carbon, as the scattering is more sensitive to pi-bonds in carbon network. One reported peak is at 1575cm^{-1} attributed to the E_2g_2 mode (the bond stretching of all pairs of sp^2 atoms in both rings and chains), referred to as the G peak. Another one is found at 1355cm^{-1} corresponding to the breathing modes of rings, referred to as the D peak [Ref: Ferrari AC, ibid; Schwan J, et al. ibid].

In the present case, both G and D peaks appear. However, no attempt is done to compare the relative intensities, as it requires deconvolution of the spectrum to deduce the quantitative information. The deconvolution process may not be precise due to the

broadening of the respective peaks. The broadening observed in the G and D peaks in amorphous diamond like carbon depends on the size of clusters, their distribution, chemical environment and stress in the film. The existence of the D peak is considered to be the evidence for benzene or condensed benzene rings in amorphous hydrogenated carbon films. The G peak is not necessarily composed of the E_2g_2 mode of graphite alone but also of sp^2 C=C stretch vibrations. [Ref: Schwan J et al., ibid]. The interpretation of the G and D peaks is complicated in DLC. Unless done in conjunction with some other technique, Raman analysis appears useful only for qualitative information.

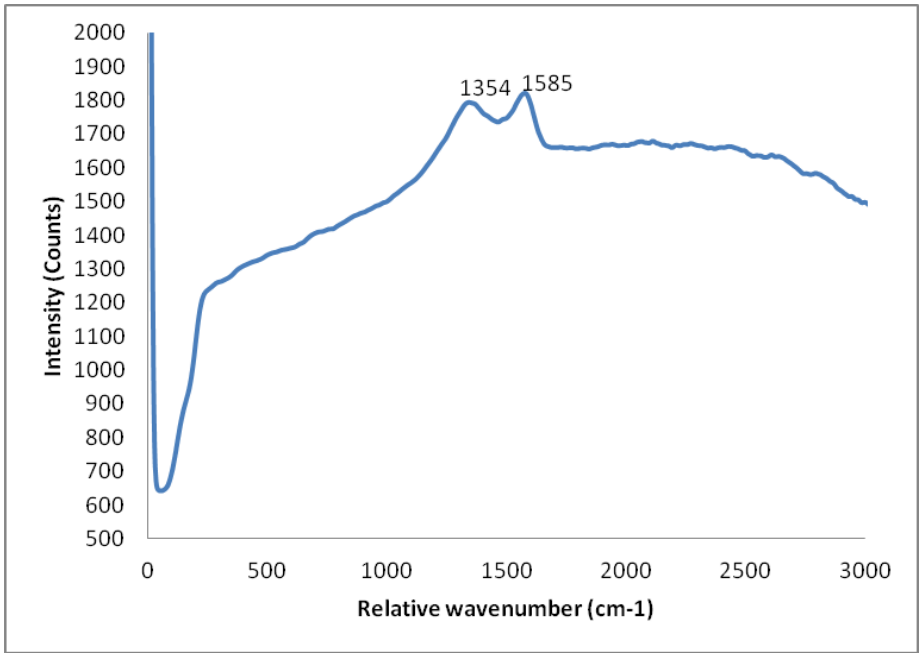

Figure 3. Raman spectrum taken on the surface of the coating on the Printed Ti sample.

X-ray photoelectron spectroscopy (XPS) analysis of the DLC coating surface was performed on SAGE model spectrometer (SPECS GmbH) with Phoibos 100MCD for Electron Energy Analysis. Peaks were recorded with constant pass energy of 40eV. Peak around 285eV will indicate the presence of carbon, deconvolution of which helps to identify sp^2 carbon (positioned at 284.8 eV) and sp3 carbon (positioned at 285.7eV) quantitatively.

The XPS spectrum (taken using MgK-alpha radiation of energy 1253.6eV) showed a peak around 285 eV indicating the presence of carbon (C1s peak). A deconvolution was done to identify sp^2 carbon (positioned at 284.8eV) and sp^3 carbon (positioned at 285.7eV). The quantities of these species were calculated to be 79.1% and 20.9% respectively (Figure 4). This ratio is very typical with diamond-like carbon.

The optical Profilometer image showed a highly homogeneous surface without any specific growth features or defects (Figure 5). Pores were present, but in minimal numbers. The surface has a R_a value of 17.9 nm and the peak-to-peak roughness is 62.4

nm. There were no features in the scanning electron micrograph (SEM) in the submicron level. The coating appeared free from defects and discontinuities.

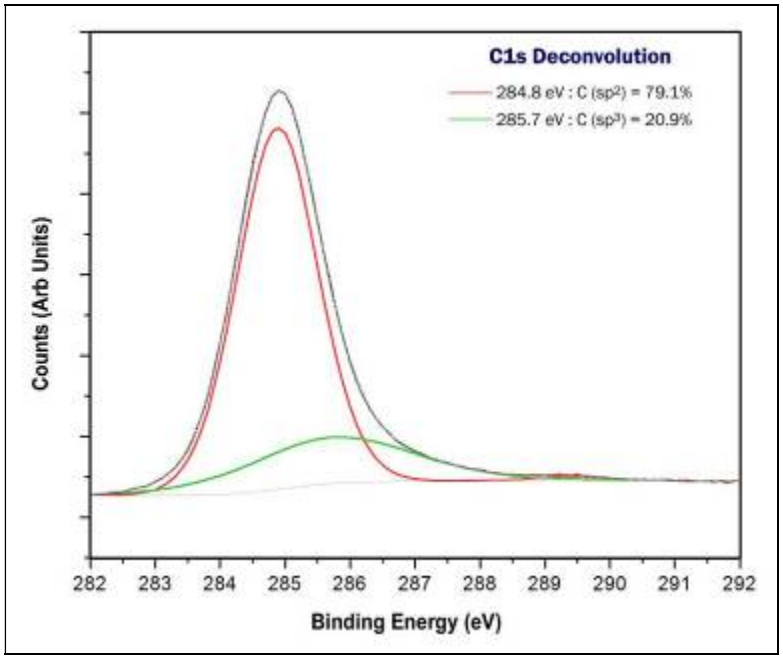

Figure 4. The C1s peak obtained in the X-ray Photoelectron Spectroscopy (XPS) of the surface of the DLC layer. The deconvoluted peaks corresponding to sp2 and sp3 species are traced underneath.

Figure 5. The surface image of the coated sample, obtained in the optical profilometer.

Adhesion strength of the coating on Ti substrate was investigated using micro-scratch method. The test has been performed in a Micro-Combi Tester. A linearly progressive normal load was applied with a Rockwell (Diamond) indenter of 100 μm radius. The starting load was 0.05 N (default value) with a loading rate of 25 N/min. Testing was performed over a scratch length of 6 mm at speed of 10 mm/min, with a final load value of 15N. The critical loads for first crack event (Lc1), first de-lamination (Lc2) and total de-lamination (Lc3) were determined from the penetration depth profile. As the friction values may fluctuate due to the presence of particle debri and local irregularities, the critical loads were reconfirmed using the acoustic data (vibrations emitted during failures). The failure events were verified the

help of optical microscopy (Figure 6). The average Lc3 for 16 measurements was 8.36 N (SD ± 0.69). The value matched with that reported for DLC in literature. A failure value of 8N is sufficient for the proposed application of orthopedic implant coating. The scratch track (observed in SEM) contained 'wedge spallations' indicating that the coating adhesion is strong enough to bear the stress faced by the implants.

The micro hardness measurements were carried out using Micro Combi Tester (CSM), wherein the coating surface was intended with Vickers triangular pyramid diamond tip under a gradually increasing normal load. The loading rate selected was 100 mN/min and at 50mN load, 10s hold time was given. The Vickers' microhardness value and the Youngs' modulus were calculated from the resulting 'load - displacement curves'

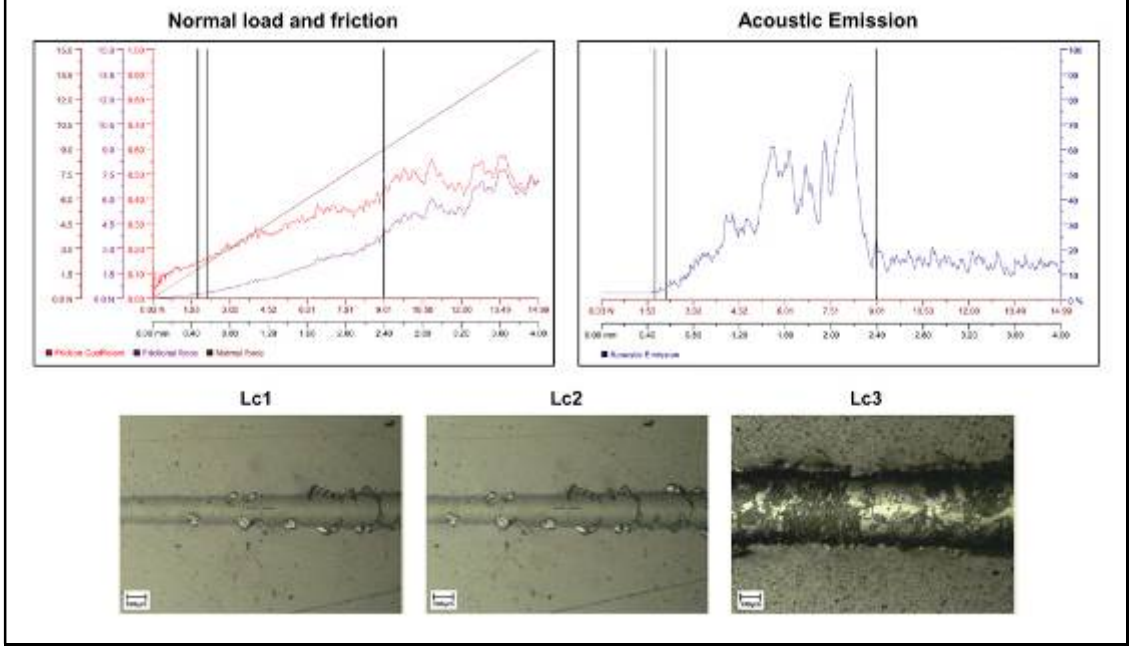

Figure 6. The results of the scratch test done on the control/comparison sample of mirror-polished titanium. Normal load and friction data, acoustic emission data and optical images corresponding to the three events are shown.

using the software. The measurements were taken on a 3x3 matrix with minimum 250μm spatial distance between indentations, and the values were averaged.

The microhardness test data with depth variation is given in Figure 7. It shows the Vickers hardness value of the coating to decrease with depth, which is observed with thin coatings. For hardness calculations, the depth of indentation should be such that the plastic deformation zone of indentation is within the coating, so as to avoid substrate effects. DLC is at least 4-5 times harder than Ti (substrate) and hence the hardness at a depth of 0.25 microns in a 1 micron coating could be taken as a reasonable estimate for the hardness of the coating. The Vickers hardness value obtained was 2913 (28.57 GPa), a reasonable estimate of the microhardness of the coating.

The modulus corresponding to these measurements in each case was calculated by the software from the load-displacement curves. The initial high value (479 GPa) reduces till a depth of 0.3 microns and stabilizes to an average of 261 GPa. The modulus value at 0.25 micrometer depth is 339 GPa.

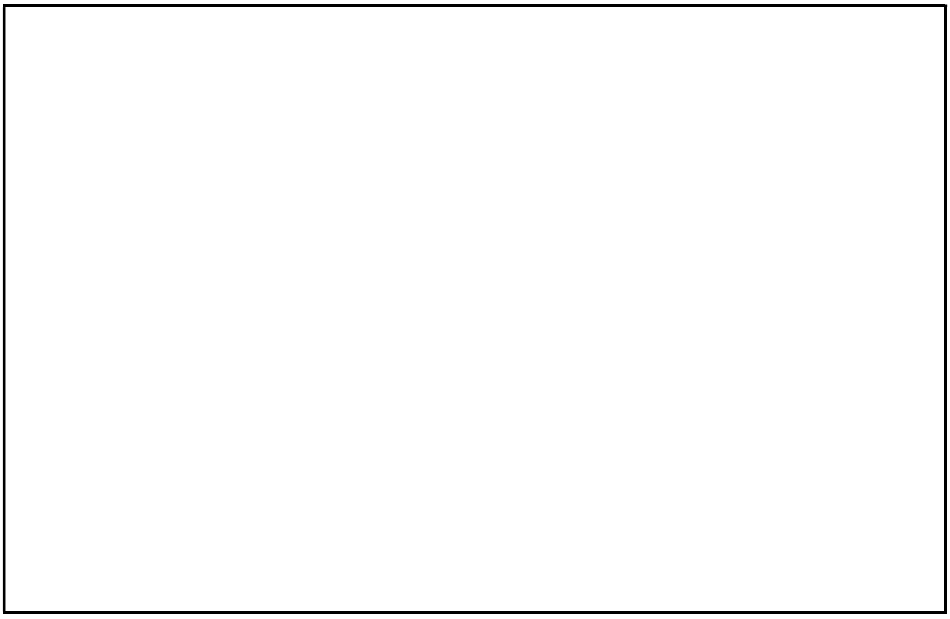

Figure 7. Depth variation of Vickers microhardness in 1 micron coating. The value at 0.25 microns (marked) is taken as the reasonable estimate for the coating hardness.

2.4 Biological evaluation of the DLC coating (*in vitro*)

The cytotoxicity of the DLC coating was studied with mouse fibroblast cells (L929, ATCC strain) in 'direct-contact' method on coated titanium discs of 12mm diameter and 1mm thick. HDPE discs were used as the negative control and stabilized PVC discs as positive control. Approximately $3x10^4$ cells were seeded per well to a 24 well plate, supplied with Eagle's MEM containing 10% fetal bovine serum. Test samples, negative controls and positive controls in six replicates were placed on the cells. After incubation at 37±1 ºC for 24 to 26h, cell monolayer was examined microscopically for the response around the test samples. The morphology of the cells in contact with the test samples was unchanged, indicating that the DLC is non-cytotoxic (Figure 8).

In the cell response study, the cells isolated from human periodontal ligament tissues (hPDL) were cultured for the tests and characterized for the progenitor cell markers (CD90, 105 and Stro-1). The hPDL cells isolated were confirmed to be positive for stem cell markers. They were cultured with DLC in an osteogenic induction medium (100 mg/mL ascorbic acid with 10mM b-glycerophosphate and 10nM dexamethasone). The ability of hPDL cells to differentiate into an osteogenic lineage was analyzed by staining using Alizarin red, Von Kossa and Masson's Trichrome (Results in figure 9).

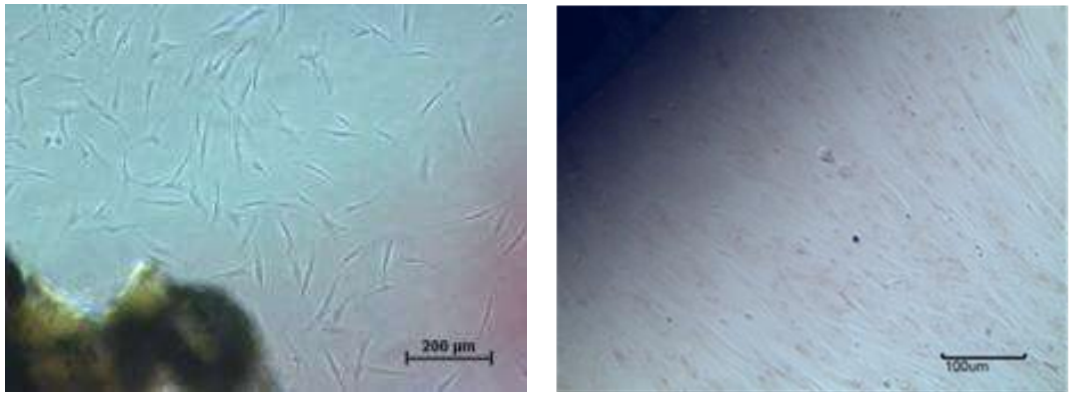

Figure 8. Cells cultured in contact with DLC coated samples to see the cytotoxicity. A) Mouse fibroblast cells. B) Human periodontal ligament cells.

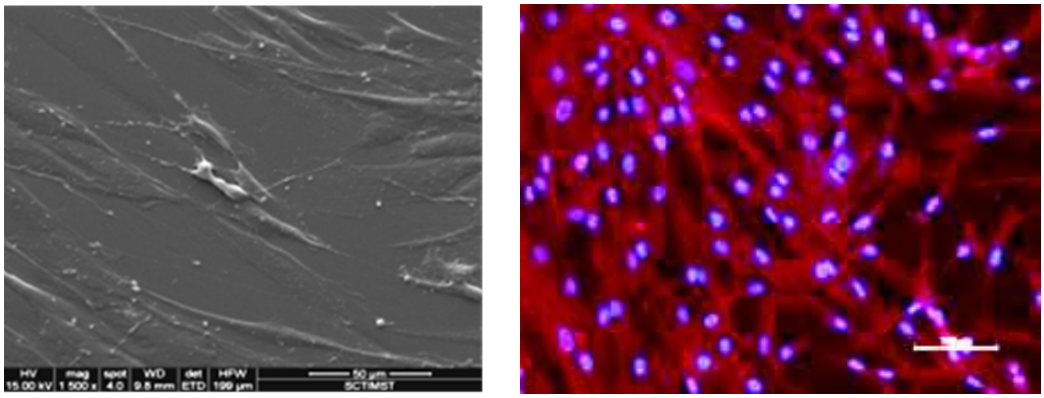

Figure 9. Human periodontal ligament cells grown on DLC. A) SEM picture showing the morphology. B) Same culture stained for actin filaments and nucleus.

Observations on cell adhesion and spreading in SEM indicated the cyto-compatibility of DLC. The induction of hPDL cells into osteogenic lineage in presence of DLC was evident from the calcium deposition identified by positive staining. It is clear that DLC has not inhibited the osteogenic potential of hPDL cells. The study proves DLC to be an ideal coating for implants to impart cell compatibility.

2.5 Bacterial adhesion studies on DLC coated titanium surfaces.

Four microbial strains were used for the study - *S. epidermidis* ATCC 35984, *Staphylococcus aureus ATCC 25923, Escherichia coli ATCC 25922*, and *Candida albicans 10231* and Methicillin resistant *S. aureus* (ATCC 700698). These were preserved at -70◦C in glycerol broth (85% Nutrient broth and 85 %Glycerol) and revived on requirement by sub-culturing into Tryptone Soy Agar (TSA) for 18-24h at 37±1◦C. The incubation throughout the study is done in a shaker incubator at 37±1◦C, with 100 rpm shaking. Titanium discs of 20mm diameter and 4mm thick were coated with DLC. 6 numbers each were made for each microbial strain. Uncoated titanium discs were used as control.

The samples (DLC coated and uncoated titanium discs) were transferred into Tryptone Soy Broth (TSB) in separate containers and incubated at for 1 hour. Two to three colonies from TSA were sub-cultured into Tryptone Soy Broth (TSB) and incubated for 1 hour. It was then inoculated into the flasks containing DLC coated and uncoated titanium discs so as to get an initial inoculum density of 10^5 cfu/ml, and incubated for 7 days. Then the inoculum was removed and titanium discs were washed thrice with PBS to elute non-adhered bacteria. The titanium discs were then transferred to glass test tubes, in which a measured volume of Phosphate buffered saline (PBS) was added so as to immerse the titanium discs. The adhered bacteria were removed by sonication and vortexing. The PBS suspension of bacteria was inoculated into TSA and incubated for 18-24 hours. The number of colony formed on TSA after incubation period was counted and the number of bacteria adhered was calculated. Determination of viable count was done in triplicates and statistical significance evaluated using Student's T-test.

The results of the counting of various strain on uncoated titanium discs and Diamond like Carbon (DLC) coated discs at 7 days period are presented in Figure 10.

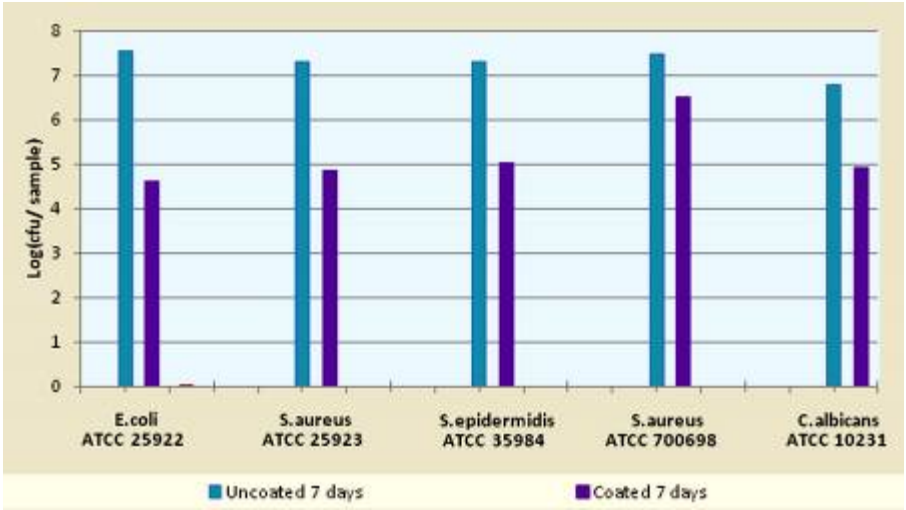

Figure 10. Graph showing the adhesion pattern (Log [cfu/sample]) of *E.coli*, *S. aureus*, *S.epidermidis*, *S. aureus* and *C.albicans* on uncoated titanium discs and Diamond like Carbon (DLC) coated discs. The reduction values are in logarithmic scale.

The significant reduction in the counts on coated sample, with respect to uncoated discs, is evident from the data. The values shown in figure 10 are in logarithmic scale. A drastic reduction of 3-orders of magnitude is seen in the case of E. coli. The reduction of *S.aureus* was least.

Separate set of samples were processed for the scanning electron microscopic (SEM) analysis. After the period of incubation of bacterial culture, the titanium discs were removed and gently washed to remove loosely attached bacteria. They were then transferred to 2.5% Gluteraldehyde for fixation and subsequently dehydrated by several passages in ethanol-water solutions for 20 min each using increasing concentrations of

ethanol up to 100%. The samples were mounted in FEI Quanta ESEM, after critical point drying and sputter coating with gold. Each strain with typical morphology, was identified in all the samples. The DLC coated samples showed considerable reduction in the SEM pictures. A representative result, with E coli strain, is presented in Figure 11.

This study shows that DLC coating can significantly retard bacterial adhesion. It opens up a scope of using the coating to prevent bacterial adhesion on implantable metallic devices. Preventing bacterial adhesion will reduce post-implantation infection in the peri-prosthetic area.

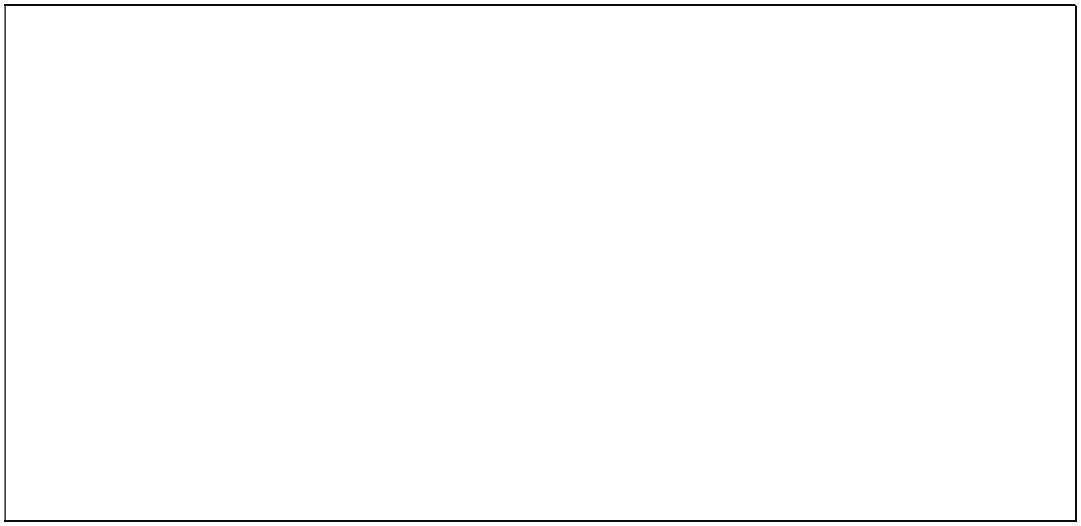

Figure 11. SEM micrographs of microbial adhesion using E-coli strains (a) on uncoated titanium discs and (b) on Diamond-like Carbon coated titanium samples.

2.6 The scope of DLC coating over titanium in the case of dental implants.

As a conclusion of the work presented in this part, it was possible to develop a hard and adherent layer of Diamond-like Carbon over titanium surface using a dedicated PECVD system. The structure, composition and physico-mechanical properties of the coating have been analysed. DLC of the obtained quality will as a protective layer against wear and physico-chemical corrosion. It has been identified that the coating is compatible with mouse fibroblast cells and human periodontal cells. In addition, it resisted the growth of bacterial strains.

The DLC coating, thus, qualifies for coating over implantable metallic surfaces. Specifically, a coating of DLC on the abutment part in dental implant system will resist the wear and biofilm formation in the oral environment.

3. DEVELOPMENT OF HYDROXYAPATITE COATINGS

3.1 Basic principles of Pulsed Laser Deposition

The coating technique 'Pulsed laser deposition' (PLD) involves the physical transfer of a material in molecular or micro-crystalline form dislodged from a target surface using laser energy, on to a substrate surface. This process is conducted in high vacuum (without any gas environment) to get a pure material coating, or in the presence of a background gas (such as oxygen) to get a reactive product layer. A high-power pulsed laser beam is focused inside a vacuum chamber to strike a target of the material that is to be deposited and substrate on which coating to be formed is kept facing the target. The material get vaporized (or 'ablated') with minimal disintegration, and emanate from the target in a 'plasma plume'. Compared to other physical vapour deposition/coating techniques, PLD has the advantage of keeping the stoichiometry of the materials if it is a compound or mineral, along with high throughput. Therefore, PLD is used widely in industry to coat ceramic materials on to metallic/solid substrates. In biomedical area, PLD is commercially applied for coating bioceramic materials on metallic implants.

A schematic of the experimental arrangement of PLD is given in figure 12. Despite the apparent simplicity in the coating system, the physical phenomena of laser-target interaction and the film growth are quite complex.

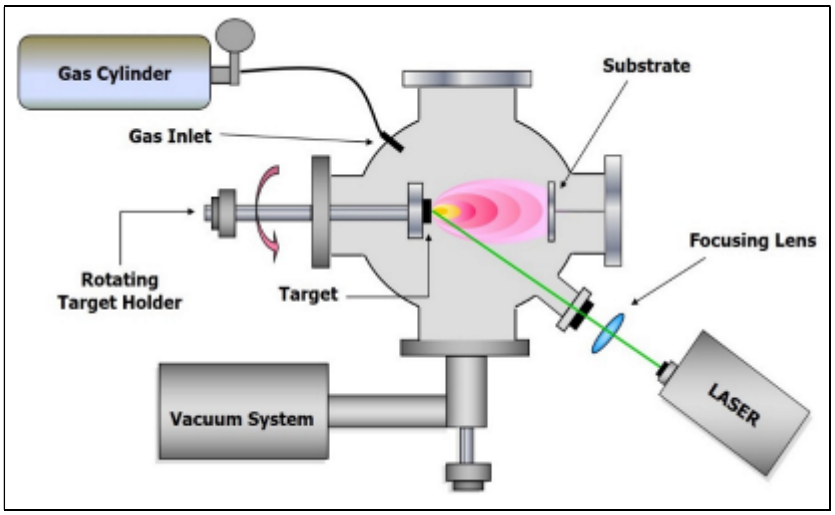

Figure 12. Schematic of the Pulsed Laser Deposition System.

In the present work, an in-house developed PLD system with a similar layout is used. It has the provision of holding multiple target (so as to make multi-layer coatings) and batch sample loading, with rotation and heating facilities inside the chamber.

The crucial part in the PLD technique is the preparation of the substrate (the surface to be coated) and preparation of the target, to have coatings of appropriate quality. These details are given in the following sections.

3.2 Preparation of the substrate and the target

3.2.1 Titanium substrate preparation

Commercially available Ti6Al4V sheets and rods (Grade2, ASTM F67, Unalloyed Titanium for surgical implant applications) were machined into different dimensions. The samples were mechanically polished (Buehler-Ecomet 3 Variable speed Grinder-Polisher, Buehler Ltd, U.S.A) progressively from 240 to 600 grit SiC emery paper to remove macro–level surface defects, contamination and to make a uniform surface. Finally, micron sized alumina suspension was used to obtain high level surface finish (~0.15mu R_a value). The polished samples were ultrasonically cleaned in de-ionized water, ethanol and in acetone.

3.2.2 Target preparation

Hydroxyapatite (HA) powder was synthesised by wet precipitation technique by the reaction between calcium nitrate and ammonium dihydrogen phosphate (Rankem, India) in Ca/P stoichiometric proportions of 1.67 at a pH 11 and at 80^{o}C. After aged for 24h the precipitate was washed with distilled water to remove soluble nitrates and ammonium ions. Obtained filter cake was freeze-dried, oven dried, and calcined at 300^{o}C for 2h. HA powder was pulverized and sieved to achieve particle size less than 125 µm.

HA powder of size 125microns were first compacted at low pressure in a uniaxial press (SPEX, X-Press 3630, USA) to obtain a disc shape and then compacted using a cold isostatic press (Cold Isostatic Press, EPSI, Belgium). In the cold isostatic press, a uniform pressure from all sides can be obtained through out the sample surface. The compacted discs taken out were sintered in a high temperature furnace.

3.3 Laser deposition of Hydroxyapatite

The initial process optimization of laser deposition was carried out by sintered hydroxyapatite (HA) as the target material. The process conditions can affect the quality of films/deposits produced, its crystallinity, micro-morphology, density, stoichiometry, deposition rate, mechanical properties of coating, etc. Most of the parameters were varied and optimized the appropriate condition for stable surface coating. The ablation of HA was performed with different lasers - 532, 355 and 266nm under same experimental conditions. Depositions were further carried out by 355nm laser, and varied the laser power to understand the effect of laser power density on ablation of HA ceramic under the same experimental conditions. Process efficiency was understood by thickness measurement, weight gain, surface roughness etc. The deposits were then analysed for the physico-chemical characteristics, micro morphology, the crystallite size variation, micro- indentation hardness etc.

3.4 Characterization

3.4.1 X-ray diffraction analysis

The phase purity of crystals of HA was analyzed by XRD (D8 Advance, Bruker Germany) using CuKα1 radiation operating at 40kV and 30mA current strength. The crystal structure was determined by analyzing the position and intensities of the diffraction peaks typically observed in the range of diffraction angle 2θ = 20–50^{o}.

XRD analysis confirms the use of crystalline phase pure sintered HA as the target for PLD. The pattern shown in Figure 13(a) consists of all the peaks in standard HA (JCPDS # 09-0432). The narrow peaks of HA indicated high level of crystallinity. The only crystalline phase present was HA, which was in good agreement with standard pattern for HA.

3.4.2 FTIR analysis

The Fourier Transform Infrared (FTIR) spectra of the samples were collected using a Thermo-Nicolet 5700 spectrometer. As the ceramic powder was found to be opaque to IR, the diffuse reflectance (DRIFT) technique was used for measurement. Samples were dried and the powder thus obtained was thoroughly mixed with IR grade KBr powder and the reflectance spectrum recorded in the range of 400 to 4000 cm^{-1} at a resolution of 4 cm^{-1}. KBr powder alone was used for background spectra.

The FTIR spectrum of HA target is shown in Figure 13(b). The spectra clearly illustrate various peaks correspond to hydroxyl and phosphate groups of synthetic HA. Hydroxyl stretching is observed at 3570cm^{-1} in the spectra of sintered HA target. All the theoretically predicted vibrational modes for phosphate group n1 to n4 were present in the prepared HA as well as HA coated Cp-Ti. The characteristics peaks confirm the phase pure deposition of HA over Ti surface via PLD technique.

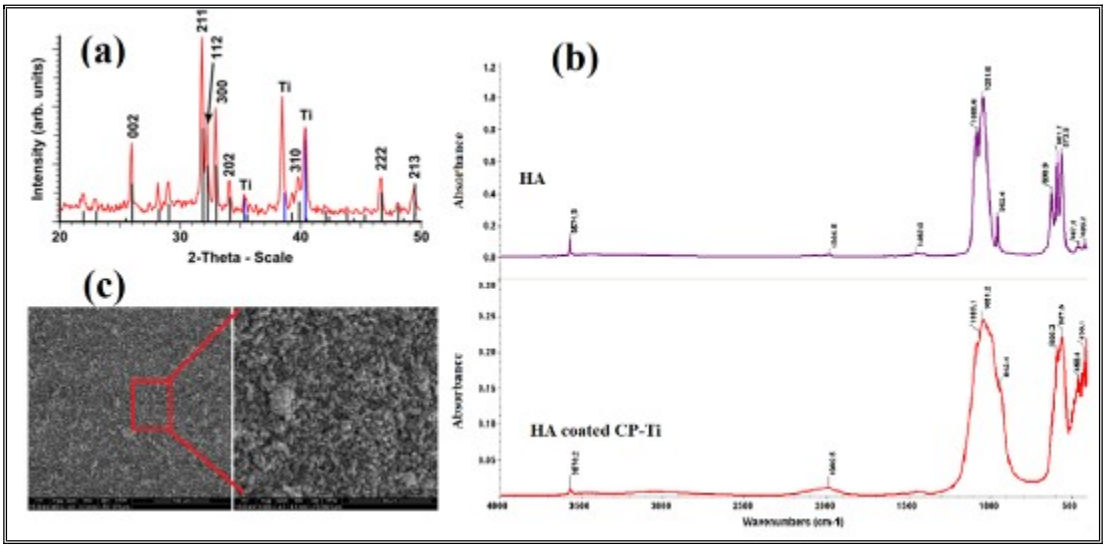

Figure 13. Results of the characterization of the hydroxyapatite coating (a) X-ray diffraction pattern, (b) FTIR pattern of sintered HA powder and HA coating and (c) SEM images.

3.4.3 Scanning Electron microscopy

The micro-scale morphology of the coating was investigated with the aid of ESEM (Quanta 200, FEI Netherlands). The disc shaped Cp-Ti samples deposited with HA layer were coated with thin layer gold for the electron microscopy. The images in different magnifications could be found in Figure 13(c). The dense packing of HA particles were seen and the distribution over the Ti surface is uniform.

3.5 *In vitro* biocompatibility evaluation on HA coating

3.5.1 Direct contact cytotoxicity test

The *in vitro* cytotoxicity test through the 'Direct contact method' serves as the first level screening for toxic potential of a material. As per ISO 10993-5 standard, the *in vitro* cytotoxicity test is done by culturing the material along with mouse fibroblast cell line (L929) and grading the reaction of the cells.

For the test, commercially pure titanium samples were prepared in the form of discs and coated with HA coated (Ti-HA). The fibroblast L929 cells were cultured in cell culture wells to form a monolayer by replacing the culture medium at regular interval. Test samples, negative controls and positive controls in triplicate were placed on the cells. After incubation at 37±1°C for 24 to 26h, cell monolayer was examined microscopically for the response at the periphery of the samples. The microscopic image is given as figure 14.

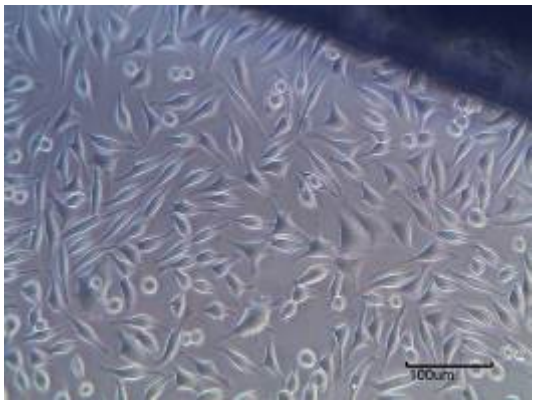

Figure 14. Mouse fibroblast (L929) cells cultured in contact with HA to see the cytotoxicity

The reactivity were graded as 0, 1, 2, 3 and 4 based on zone of lysis, vacuolization, detachment and membrane disintegration as per the table given below. The appearance of numerical grade more than 2 is considered as cytotoxic .

No.	Sample	Grade	Reactivity
1	Negative Control	0	None
2	Positive Control	4	Severe
3	Ti-HA sample	0	None

Since the test material HA coated Cp-Ti (sample code Ti-HA) achieved a numerical grade 0, the material is considered as non-cytotoxic. Negative control gave none cytotoxic reactivity and positive control gave severe cytotoxic reactivity as expected.

3.5.2 Cytocompatibility evaluation using HOS cells

In vitro cell compatibility was studied on the HA coated titanium samples. HOS (human osteosarcoma) cells were cultured in Dulbecco's Modified Eagle Medium-High Glucose (DMEM-HG) with 10% fetal bovine serum (FBS), 50 units per ml of penicillin and 50 mg/ml of streptomycin. Cells were seeded and maintained at 37^{o}C and 5% CO_2 atmosphere and experiments were performed at 80% confluence.

The samples for evaluation were conditioned in DMEM- HG (Dulbecco's Modified Eagle's Medium, Invitrogen) 10% FBS, 1% Ab (Fetal Bovine Serum and Antibiotics, Invitrogen), for 24 hours. Approximately 1x10^4 HOS cells were seeded on the scaffolds and placed at 37°C, 5% CO_2 in the incubator for 24 hours. After culturing, the samples were prepared for SEM analysis by rinsing with sterile PBS (Sigma) and fixing in 3% gluteraldehyde solution (Electron Microscopy Sciences). They were then dehydrated in ascending grades of alcohol (70%, 80%, 95% and 100%), washed with isoamyl alcohol and subjected to critical point drying. The dried samples were then gold coated and observed under SEM.

The morphology of cells in contact with HA coated Ti as seen in the SEM are shown in figure 15. The cells on HA coating showed good adhesion and proliferation. During the culture period, the cells proliferated and almost covered the surface (figure 15b). This is an indication of the bioactivity of the HA coating on Ti surface.

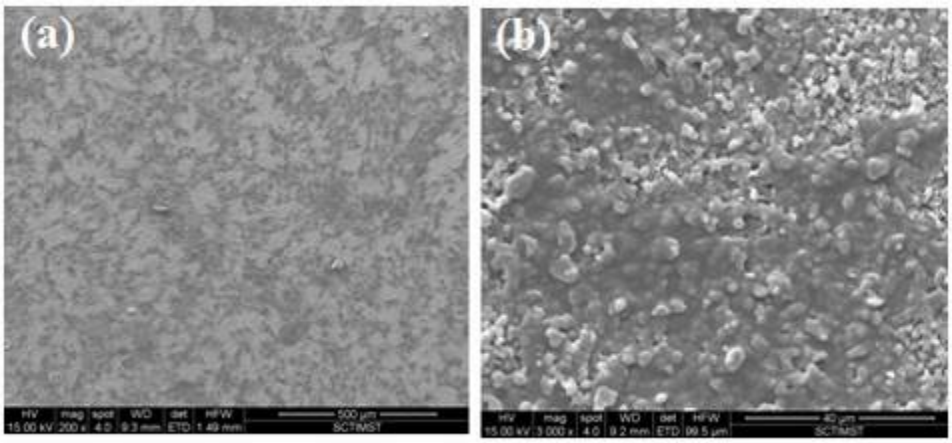

Figure 15. ESEM morphology of HOS cells attached on HA coated Ti samples (a) low magnification and (b) high magnification.

Further investigation of the compatibility of the cells with the coated surface, was done through actin and nuclear staining. Actins are an essential component of the cytoskeleton, with critical roles in a wide range of cellular processes, including cell migration, cell division, and the regulation of gene expression. These functions are attributed to the ability of actin to form filaments (the 'f-actin') that can rapidly assemble and disassemble according to the needs of the cell.

For the evaluation, the monolayered HOS cells grown over HA-coated Ti samples after 24h culture, were fixed in 3.7% paraformaldehyde and permeabilized with 0.25% Triton X-100. F-actin was stained with Alexa-fluor-488-phalloidin and the nucleus was counterstained with 4',6-diamidino-2-phenylindole (DAPI). The stained HOS cells were investigated using a confocal laser scanning microscope (Carl Zeiss LSM 510 META equipped with differential interference contrast optics). Images of the samples were prepared in multi-track mode with separate excitation of DAPI and Alexa-fluor-488-phalloidin.

Figure 16 shows the cLSM images of dual staining of actin filaments and nuclei images superimposed. It is identifiable that the actin filaments are intensely stained and thickly bundled which is the indication of remarkable expression of f-actin on the HOS cells in contact with HA coated surface. Nuclear counterstaining shows the cells are thickly populated, endorsing that the layer seen in SEM are composed of live cells. It is a known fact that β-actin (stained by phalloidin) is enriched at the leading edge of migrating cells. In the image, most of the actin filament formations are longer than 20 micrometers. These are the evidences of the high level of cytocompatibility.

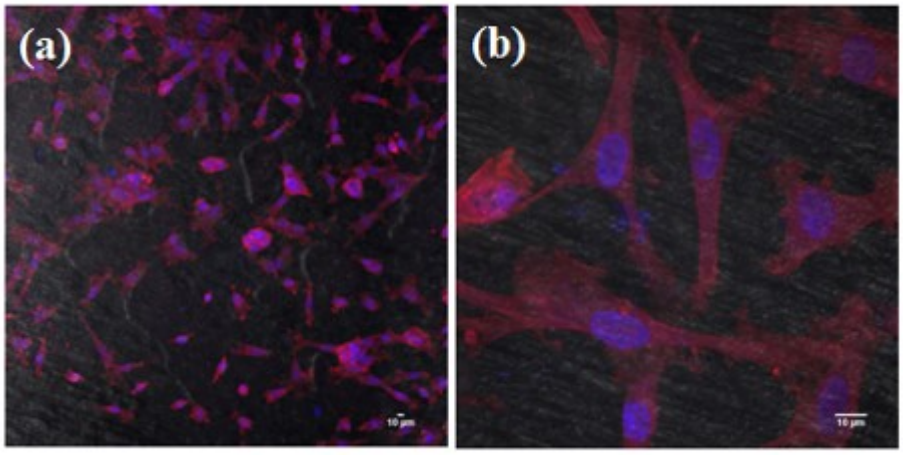

Figure 16. Images of cLSM showing the HOS cells over HA coated Ti samples stained with phalloidin and DAPI, in different magnifications.

4. ALTERNATIVE STRATEGIES FOR OBTAINING BIOACTIVE TITANIUM

The objective of developing techniques for ceramic coated dental implants has been extended so as to explore the possibilities of imparting bioactivity to titanium implant surface for achieving *in vivo* osseointegration. Two strategies were tried – one is the coating of alpha-Tricalcium Phosphate through PLD technique and the other is grafting calcium ions onto titanium surface through Hydrothermal technique.

In the original plan, the material suggested was hydroxyapatite, which is basically bone mineral composition. This choice was based on the clinical success of the material. There are other calcium phosphate materials which show higher bioactivity like tri-calcium phosphate (α-TCP). This may lead to faster integration of the local bone. Coating with α-TCP by PLD will be interesting to investigate, as a better alternative to hydroxyapatite to establish osseointegration.

The PLD technique is adopted in this project work as an alternative to plasma spray technique. As demonstrated, the PLD coating is thinner, more adherent and uniform. Yet, it is a known fact that any surface containing calcium ions may initiate the physiological process of osseointegration. Therefore it would be worthwhile to look into the possibility of attaching calcium ions onto titanium surface. Hydrothermal processing in calcium hydroxide is tried in the present work.

4.1 Tricalcium Phosphate (TCP) Coatings

4.1.1 Synthesis of α-Tricalcium Phosphate Target

The first step is to synthesize tricalcium phosphate powder by the wet reaction between calcium nitrate and ammonium dihydrogen phosphate at a Ca/P stoichiometry of 1.5 at 60°C. At this thermodynamic condition, the beta-phase tricalcium phosphate (β-TCP) will be formed. To obtain the alpha tricalcium phosphate (α-TCP), a high temperature heating and fast temperature quenching are needed. The precipitate obtained in the synthesis was dried and the powder was compacted in a uniaxial hydraulic press at 10 ton pressure. This was subjected to a heating at 1250^{o}C maximum heating rate of 2°C/min. The heating will lead to phase conversion as well as sintering. The pellet was kept at the sintering temperature for 2h and then cooled rapidly to obtain α-TCP laser ablation target. It was then surface-polished and used for PLD coating.

4.1.2 Analysis of α-Tricalcium Phosphate Coating

The coatings were done on titanium substrates of 12mm dia, after polishing and cleaning. The phase purity of the coating was analyzed by XRD (Bruker, D8 Advance) using CuKα_1 radiation operating at the tube parameters of 40kV and 30mA. The diffraction data in the range 20–70^{o} two-theta were recorded and compared with ICDD Powder Diffraction Data of TCP (Figure 17).

The XRD data shows that the coating corresponds to ICDD PDF No. 00-009-0169. α-TCP target is well crystallized without any additional phases. To verify the phase formation, the sample surface was subjected to Fourier transform infrared (FTIR) analysis (Thermo-Nicolet 5700 spectrometer) in the diffuse reflectance (DRIFT) mode. Samples were kept on the holder and the reflectance spectrum was recorded.

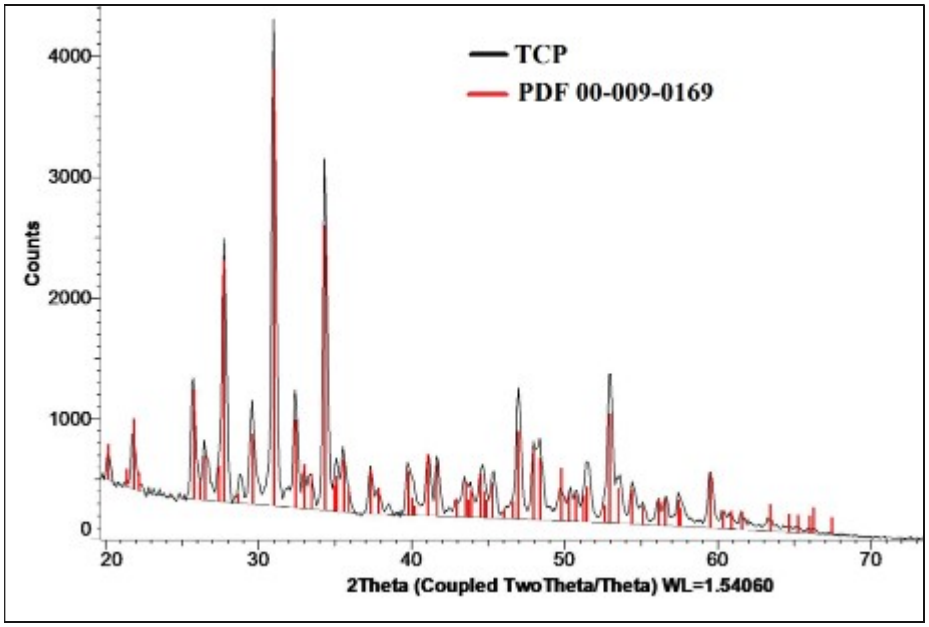

Figure 17. X-ray diffraction pattern of sintered tricalcium phosphate target. The pattern of TCP, PDF No. 00-009-0169, is also shown.

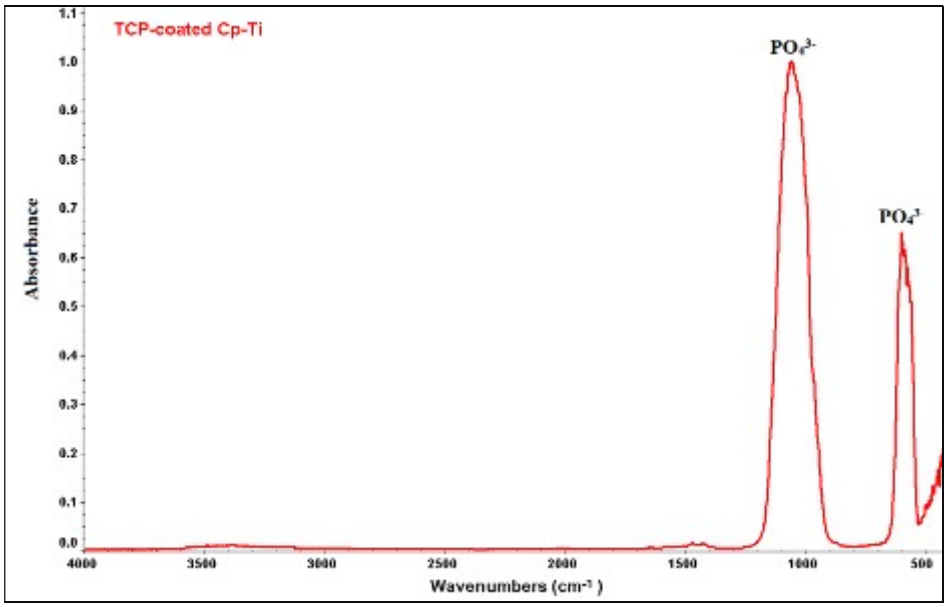

Figure 18. FTIR pattern of TCP coated over Cp-Ti using PLD.

Figure 18 shows the FTIR spectra of the α-TCP coating deposited on Ti samples. The only functional group present in TCP is the phosphate. Well defined phosphate bands are present in the region 1030-1090cm^{-1} was assigned to P-O vibration of PO_4^{3-} (v_3, asymmetric stretching of P-O bond) and O-P-O v_4 vibration mode of phosphate.

The surface morphology of α-TCP obtained by PLD is shown in Figure 19a. The film grown was seen to contain aggregates of irregular granular particles of 1-2 microns, coalesced to form the coating. The surface is uniform in terms of the arrangement of the deposits, but consists of spaces in between the growing regions filled by further deposition. This indicates a mixed mode of thin film growth. Figure 19b represents the calcium and phosphorous elemental composition in the EDS pattern of the deposited film, which corresponds to phase pure α-TCP.

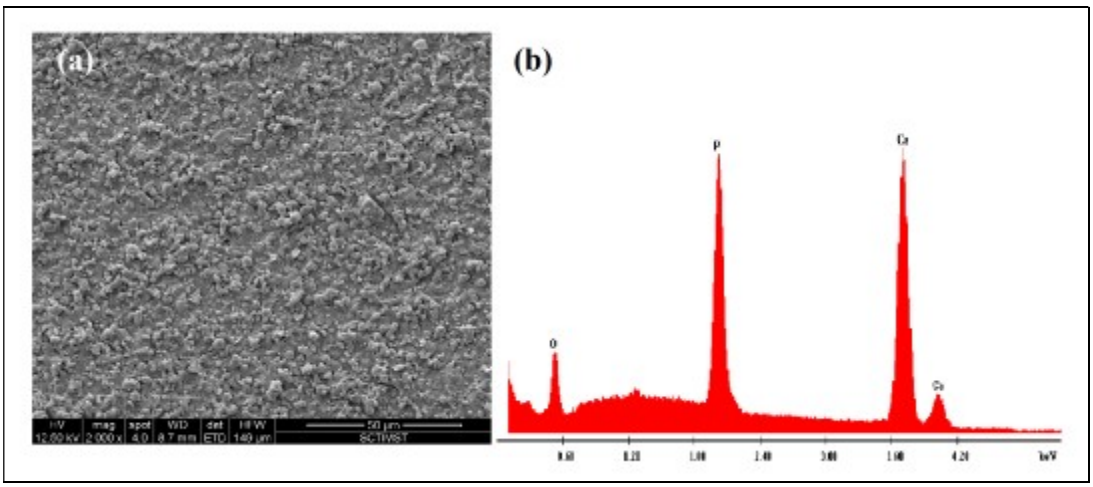

Figure 19. (a) SEM and (b) EDS images of α-TCP coated Ti sample surface.

4.2 Inducing Bioactivity to Titanium Surface

Titanium metal, due to its reactive nature, offers wide scope of modifying the surface. In this part of the work, a simple and effective technique is demonstrated, to attach calcium ions onto titanium surface through hydrothermal method. This is intended for inducing bioactivity to have better osseointegration, without the need for a thick coating.

4.2.1 Materials and Methods

Commercially pure Titanium (Cp-Ti) rods of 12 mm diameter were cut into discs of 4 mm in thickness for the use as substrate. They were polished in Buehler-Ecomet 250 machine using silicon carbide papers of 100, 250, 600 grit sizes in succession for cutting and finally with 0.5 micron alumina slurry for the final polishing. The SEM images of the polished surface are given in Figure 20A.

The substrate discs were ultrasonically cleaned in soap solution and distilled water sequentially to remove any loosely bound particles/impurities on the surface. The cleaned discs were etched by a mixture of HF (Merck) and HCl (SD Fine) prepared in the ratio 20:8 ml at 27^{o}C. HF is highly effective in dissolving the dense and stable native surface TiO_2 layer and HCl act as a good cleaning agent for removing salt deposits. The discs were subsequently sonicated in distilled water. The SEM images of the pre-treated surface are available in Figure 20B.

Figure 20. Secondary electron images of Ti sample surface of (A) polished surface (B) HF/HCl pre-treated surface.

The polishing is capable of producing smooth and flat surface, despite the presence of rare abrasion scratches and small pits. The pre-treatment or the cleaning process effectively generate microscopically rough surface by exposing the grains with sharp boundaries and edges. Also, it increases surface area of the substrate by creating pits. High surface area and roughness offer nucleation centers for the calcium phosphate to growing on titanium reactive sites, thereby improving both coverage and adhesion of the coating. The pre-treated Ti samples were hydrothermally modified using $Ca(OH)_2$ solution.

(ii) Hydrothermal treatment of Ti surface

The hydrothermal reaction was executed in a Teflon lined autoclave which has the maximum temperature and pressure ratings of 200°C and 200 bars respectively. Ti discs were treated in $Ca(OH)_2$ aqueous solution in the autoclave at 200^{o}C and at a pressure of 5 bars for over 5 h, maintaining the basic pH conditions (samples coded as Ti-HT). The processed discs were taken out, rinsed with deionised water and dried slowly in vacuum desiccators and used for further characterization and studies.

4.2.2 Physicochemical Characterization

The surface chemical changes of the hydrothermally treated Ti surface (Ti-HT) were examined using XPS (Multilab 2000, Thermo Scientific). The measurement was performed using Al-Kα radiation (1486.6 eV). The binding energies were calibrated with respect to C1s at 284.8 eV (adventitious carbon) with a precision of ±0.1 eV. XPS results

were analyzed on the basis of binding energies of Ti2p, O1s and Ca2p peaks to evaluate the chemical environment and oxidation states of the respective elements on the surface. The survey spectrum on the surfaces of Ti-HT sample is represented in Figure 21.

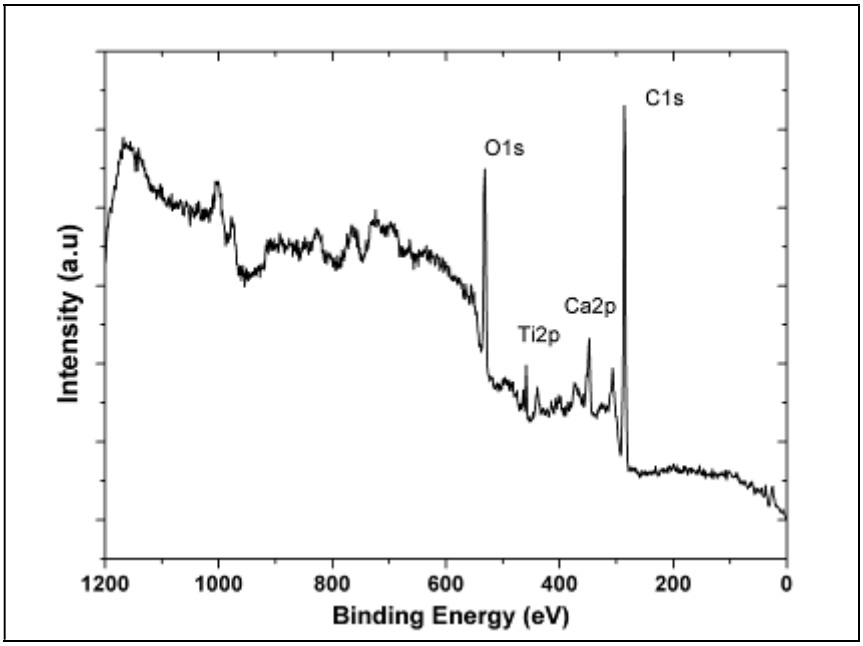

Figure 21. The binding energy survey spectrum of the Ti-HT surface.

The regions corresponding to O1s, Ca2p and Ti2p were scanned at a higher resolution, which could be found in Figure 22 (A), (B) and (C) respectively. The data obtained by the high resolution scans were analysed using Fityk, a peak fitting program. The standard binding energy values of various chemical species taken for the analysis are given in Table 1.

Table 1. High resolution XPS measurement - standard binding energies for Ca, Ti and O in different chemical environments

Element	BE (standard value, eV)
Ca $2p_{3/2}$ (CaO)	347.20
$2p_{1/2}$ (CaO)	349.80
Ca $2p_{3/2}$ ($CaTiO_3$)	346.70
Ti $2p_{3/2}$ ($CaTiO_3$)	458.87
$2p_{1/2}$ ($CaTiO_3$)	464.70
O1s (O^{2-})	529.50
O1s (OH^-)	531.50

On analyzing through curve fitting, the O1s spectrum [Fig. 22(A)] revealed that O existed in two different forms O^{2-} (529.5 eV) and OH^- (531.5 eV) on the surface of the sample. The intensity of the OH^- was higher compared to O^{2-} indicating that the content

of oxygen in $Ca(OH)_2$ is higher on the surface of the sample, which is expected due to the hydrothermal treatment with $Ca(OH)_2$. Similar analysis on Ca2p data [Fig. 22(B)], revealed that apart from $Ca(OH)_2$, Ca also exists in the form of CaO (346.7 eV) and $CaTiO_3$ (346.7eV).

However, from the relative areas of the respective peaks, it can be seen that the amount of Ca in CaO is higher than Ca in $CaTiO_3$. Since the atomic % of Ca in both the compounds is the same, it can be inferred that the amount of CaO is higher than $CaTiO_3$ on the sample surface. The presence of $CaTiO_3$ is further confirmed by the Ti2p peak data. The binding energy peak 458.87 eV corresponding to $CaTiO_3$ was observed (See Fig. 22C) and other peaks of Ti were absent indicating the surface of the sample has Ti in the form of $CaTiO_3$ as opposed to TiO_2 or unbonded Ti.

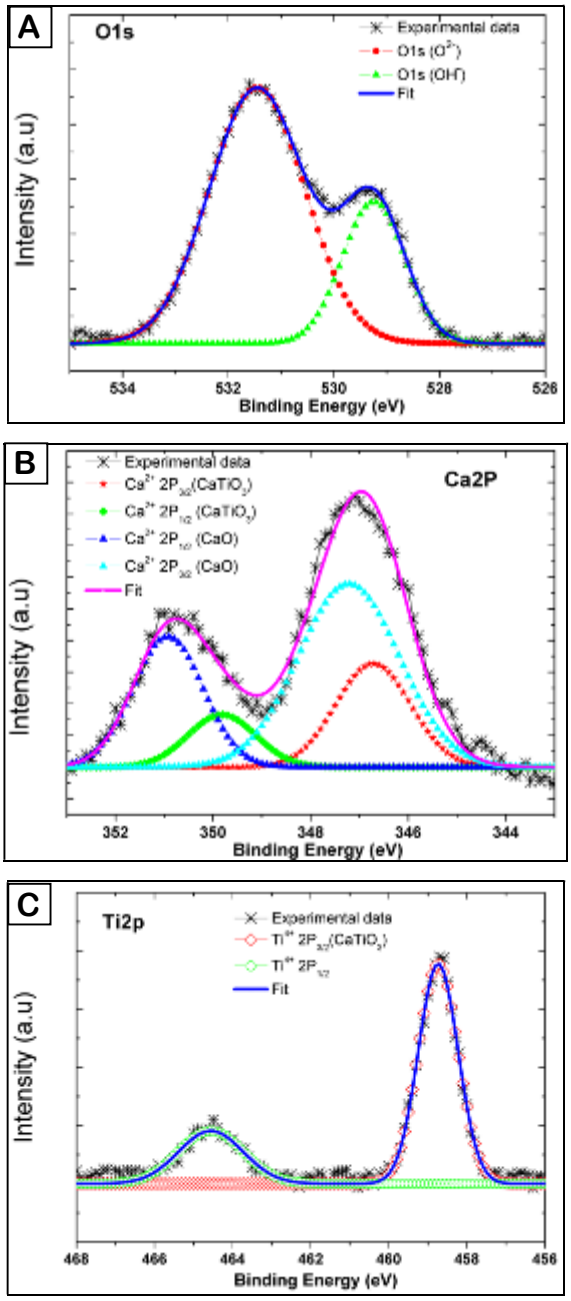

Figure 22. High resolution XPS spectra from Ti-HT surface of (A) O1s, (B) Ca2p and (C) Ti2p,along with the deconvolution of the peaks.

During the hydrothermal reaction, both the dense oxide (TiO_2) surface layer and part of Ti in the bulk which is close to the outer oxide layer are attacked by OH^- ions and dissolved into the $Ca(OH)_2$ solution. This increase the concentration of Ti^{4+}, which is followed by re-crystallization in the vicinity of Ti surface due to the lower energy of Ti-O bond. The dissolution-re-crystallization process produces large number of negative charges on the Ti surfaces which leads to the migration of Ca^{2+} ions from the solution to Ti surface and subsequent precipitation. The $CaTiO_3$ on Ti surfaces is expected to increase apatite deposition with a higher bonding strength. The presence of $CaTiO_3$ has also been shown to improve the integration and acceptance of the bone implant.

4.2.3 In vitro bioactivity studies - Evaluation of apatite deposition on Ti

The biomineralization behavior (or the apatitic calcium phosphate deposition) on the surface-modified titanium was evaluated through 'In vitro Bioactivity Test' in simulated body fluid, as per literature. A supersaturated SBF in 1.5 concentration (1.5SBF) was used for the study, in which any bioactive surface will host the nucleation and growth of calcium phosphate material. Polypropylene vials of 50 ml volume were taken and the surface-modified discs were placed one each in them. They were filled with 15 ml SBF so as to immerse the disc fully, and incubated at 37±1^{o}C. SBF was replenished every day and after the immersion periods of 1, 5 and 7 days, the discs were retrieved. They were rinsed in distilled water and dried in a vacuum desiccator. The morphology, crystallinity and phase of the depositions over Ti discs were analyzed.

The micromorphology of the deposits was assessed in SEM. The phase composition was determined using X-ray diffraction (D8 Advance, Bruker). The machine used CuKα1 radiation at 40kV voltage and 30mA current strength and the diffraction peaks were observed in the range 20–60^{o}. FTIR analysis was performed in Thermo Nicolet 5700 spectrometer to identify the functional groups on the surface. The deposited CaP from the coated surface was collected and made as thin pellet with KBr and analysed in the range 400–4000 cm^{-1} at a resolution of 4 cm^{-1}.

The SEM and images of the Ti-HT samples are shown in Figure 23. In the sample undergone 1 day of SBF soaking, some small grains with size less than 1μm in diameter were observed. During 5 days of immersion, spherical CaP growths were seen uniformly distributed on the surface. At 7 days of soaking, the apatite layer coating over Ti-HT surface was thick and with larger globular structure. On the Ti metal control surface (unprocessed), only rarefied growths were seen during the periods.

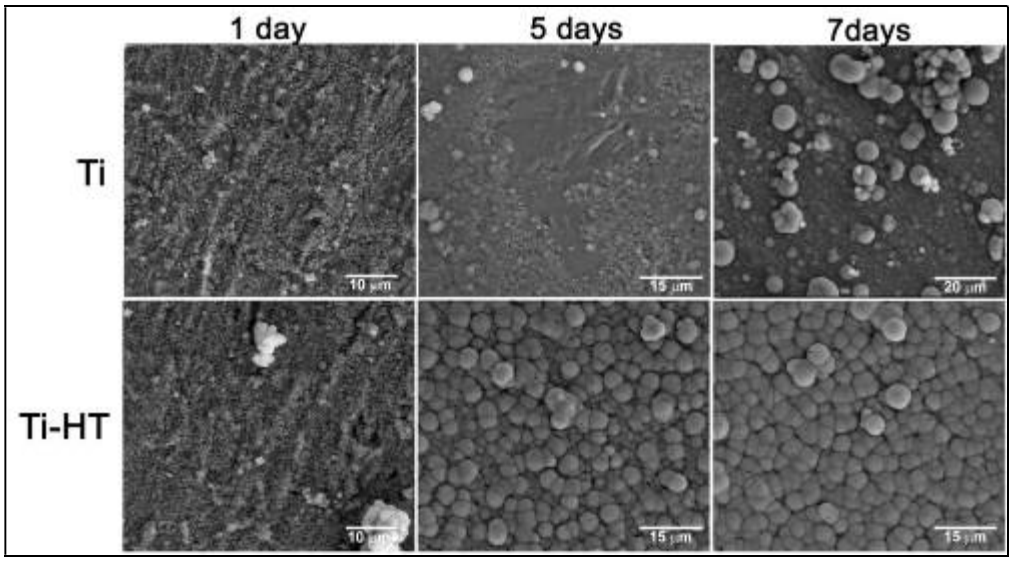

Figure 23. The SEM images of Ti and Ti-HT surfaces after immersion in SBF for 1day, 5days and 7days.

The higher magnification of SEM image at 7 days of SBF socking is shown in Figure 24 (A), which confirms the growths in typical apatite morphology. The entire surface was covered by dense and compact coating of CaP. The elemental composition of corresponding surface assessed via EDS spectra (Fig.24(B)) showed the presence of peaks of only Ca and P, wherein the Ca/P ratio is approximately 1.67. There were no traces of Ti substrate peaks indicating the higher thickness of CaP coating.

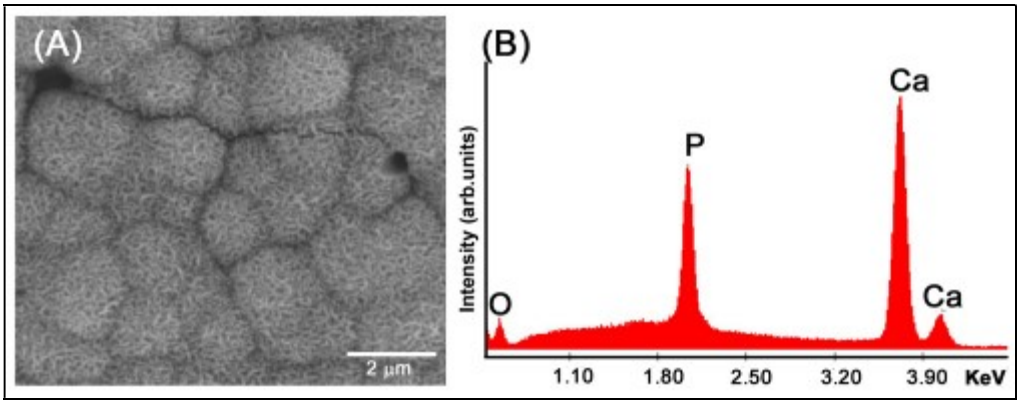

Figure 24. (A) Higher magnification of SEM images of Ti-HT surfaces after 7days immersion in SBF and (B) corresponding surface EDS spectrum.

The phase purity and chemical bonding of CaP precipitated surface assessed using XRD and FTIR techniques are represented in Figure 25. The XRD pattern (Fig. 25 (A)) revealed the formation of apatite on Ti-HT soaked in SBF for 7days, as the diffraction peaks matched with those of ICDD pattern (09-0432) of hydroxyapatite. The peaks were broad and overlapped at closely spaced peaks, indicating the nano-level domains in the apatite formed. The FTIR spectrum of sample in Fig.25 (B) contained the characteristic peaks of apatite formation and the vibrational bands of PO_4^{3-} group were observed at 1061, 597 and 563 cm^{-1}. Also the bands assigned to O-H stretching and bending were detected at 3443 and 1641 cm^{-1}, respectively. Finally, three strong CO_2^{3-} group bands, at 873, 1423 and1471 cm^{-1}, were detected. Based on the above results, it can be resolved that the CaP coating on Ti-HT is characteristic carbonated apatite.

4.2.4 In vitro cytocompatibility: Direct contact test and MTT assay

An *in vitro* cytotoxicity test of Ti and Ti-HT samples were done using direct contact test followed by MTT assay, as per ISO 10993-5. L-929 cell lines were used for the test. Test samples, negative control (Ultra high molecular weight poly ethylene) and positive control (Stabilized PVC disc) in triplicate were placed on the cultured cell monolayer. After incubation at 37±1°C for 24h, cell monolayer was examined microscopically for the response around the test samples. Microscopic observations were done to assess the effect of direct contact. Further MTT assay was performed to measure the metabolic activity of cells by observing the reduction of yellow colored tetrazolium salt 3-(4, 5-Dimethyl thiazol -2-yl)-2,5-diphenyltetrazolium bromide to purple colored formazan.

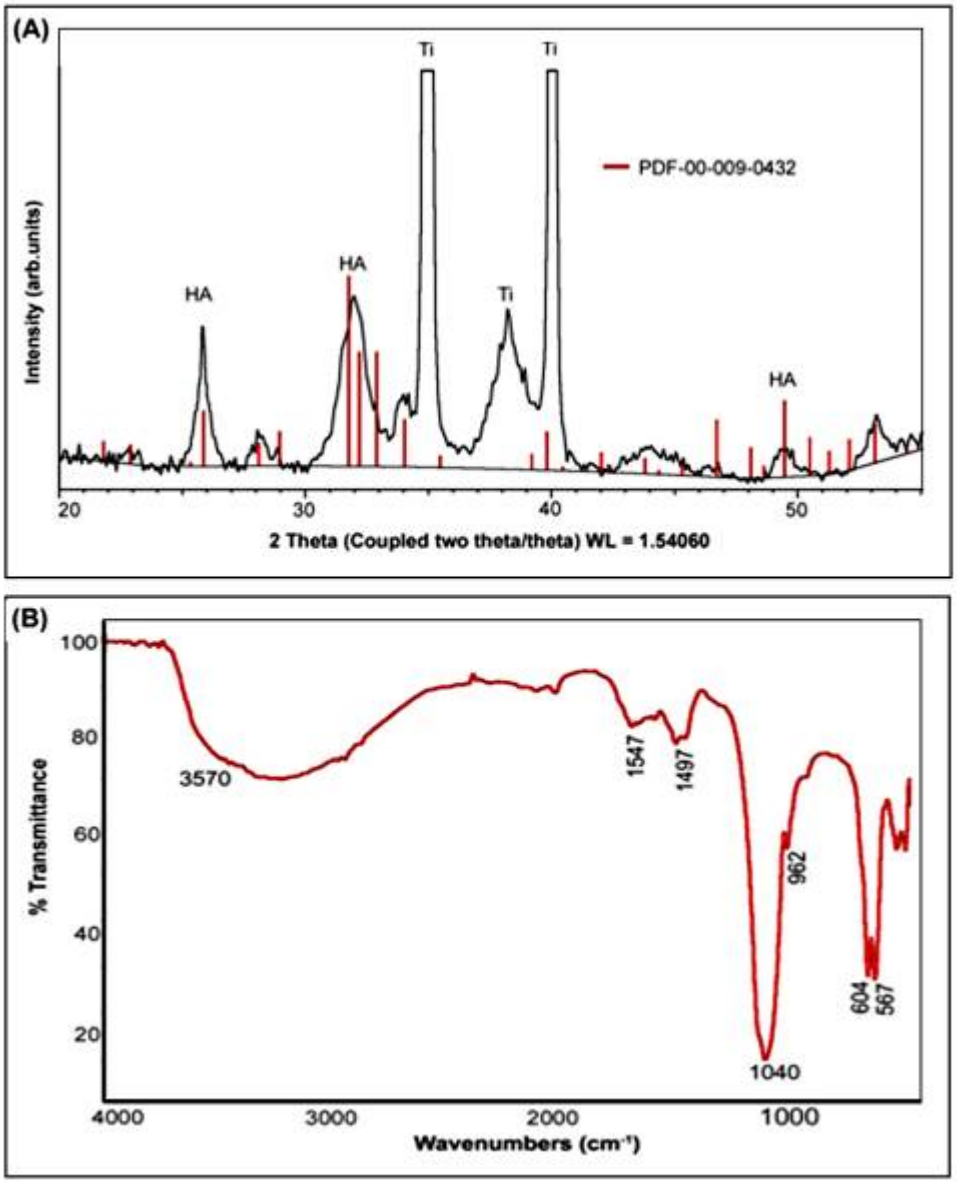

Figure 25. The phase analysis of the coating formed on Ti-HT surface in7days of immersion in SBF- (A) XRD pattern and (B) FTIR spectra.

After removing the test samples from the cell monolayer, 400µl MTT (1mg/ml in medium without supplements) solution was added to test sample and controls, and then the plates were wrapped with aluminium foil and were incubated at 37± 2°C for 2h. After discarding the MTT solution, 300µl of isopropanol was added to all wells and mixed thoroughly. The colour developed was quantified by measuring absorbance at 570 nm using a spectrophotometer. The data obtained for the test samples were compared with the data from the control material, as well as the cell control.

The images of direct contact test and the values of MTT assay are represented in the Figure 26. The cells were well attached and spread in the presence of Ti-HT and there

were no significant difference between the cells morphology, proliferation and metabolic activity with respect to the controls.

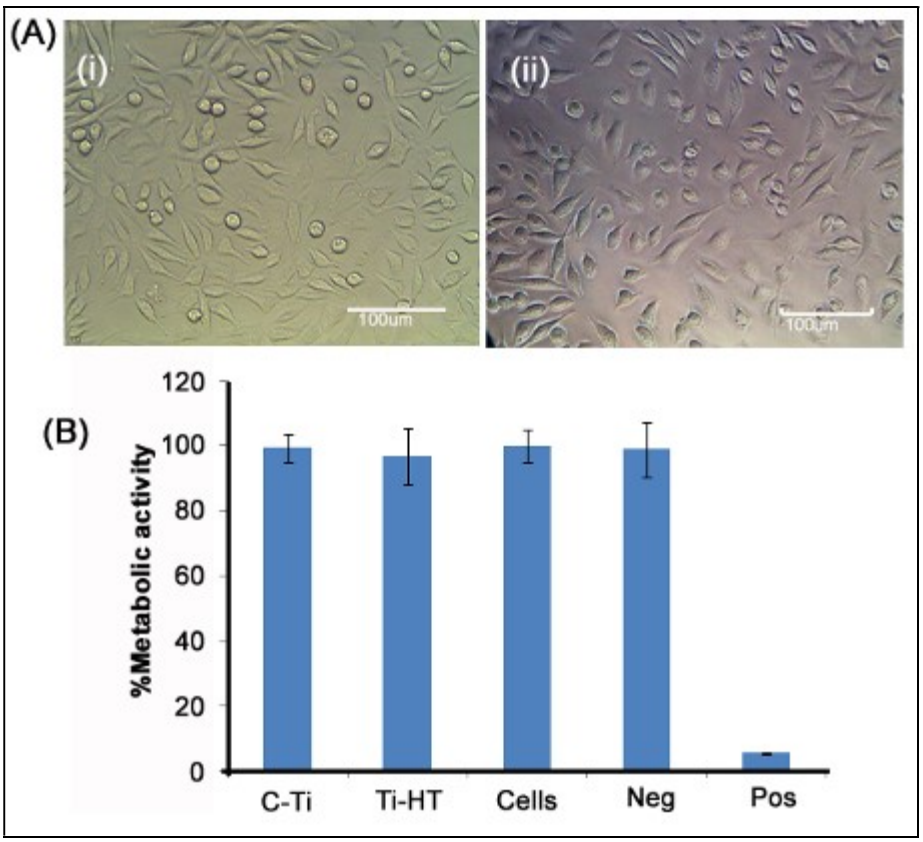

Figure 26. Cytocompatibility evaluation of titanium samples represents in 'A' direct contact method [(i) Ti and (ii) Ti-HT] and 'B' MTT assay using L929 cells.

4.2.5 Cell response – Alamar Blue Test and Cell Adhesion

The cell proliferation was investigated by culturing mouse fibroblast cells in contact with the samples (Ti and Ti-HT) and assaying using Alamar Blue (Invitrogen). Alamar blue (AB) assay converts metabolically active cells to pink color via reduction potential studies based on vitality of mitochondrial reductase enzymes.

The cells (L929 cell lines) were seeded (5000cells/well, 4 replicates per each time point) in 24 well plate and the materials placed over the cells surface. They were maintained with cell culture medium containing 10% FBS at 37^{o}C for 24 - 72 h in 24-well plates. The media were regularly changed every 2 days. Prior the assay, samples were transferred into a new 24-well plate and a fresh medium was added to all wells. Alamar blue reagent was then added at 50 µL/well followed by a further incubation for 4h. Then 100 µL was transferred from each well into a black 96-well plate (Greiner Bio-One) and fluorescence was measured immediately at 590 nm (with excitation at 560 nm) (Infinite M200 PRO Plate Reader, Tecan). The measurements are expressed in percentage activity of live cells against control (Figure 27).

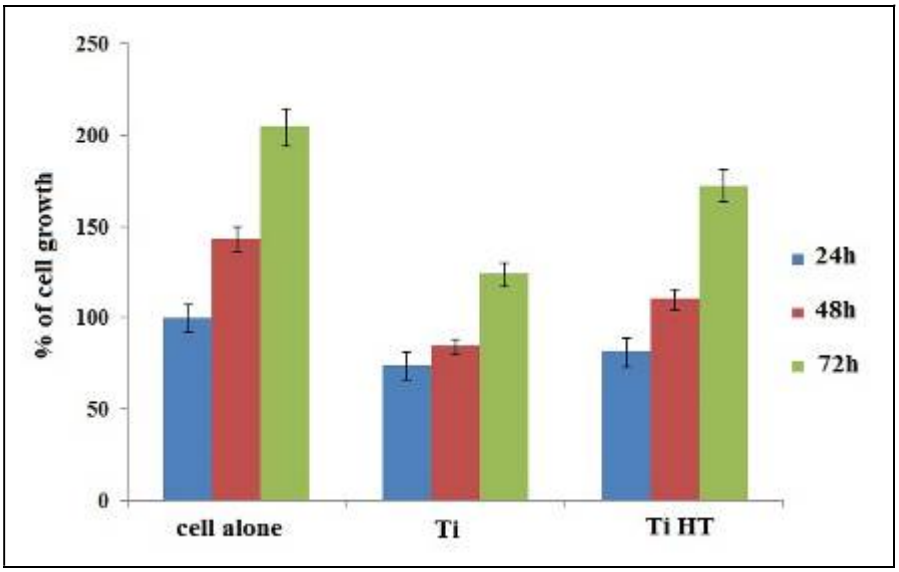

Figure 27. Cell proliferation assay (Alamar Blue test)

Cell adhesion was performed using L929 cells for 24-72h. The cells were seeded on Ti and Ti-HT surfaces (5000cells/sample surface, per each time point). Subsequently the samples were placed in 6-well tissue culture plate and maintained with a-MEM containing 10% Fetal Bovine Serum and 50units/ml of penicillin and 50mg/ml of streptomycin at 37^{o}C under 5% CO_2 atmosphere. The cell-seeded samples were retrieved after time periods 1 to 3 days, fixed in gluteraldehyde, coated with gold and examined in scanning electron microscope (SEM).

The SEM results showing cell morphology and adhesion are given in Figure 28. Ti-HT surface proves a better platform for cell adhesion compared to bare Ti. Cell proliferation is minimal at 24 hours period. On the increase of time period, the cells proliferate faster in Ti-HT surface than that of bare Ti surface. The cell proliferation density is comparable in both the surfaces, with Ti-HT surface showing better performance.

The results of the studies done on the hydrothermal processed titanium in calcium hydroxide solution indicated the formation of a calcium-rich nanolayer on the discs. This layer facilitated apatite formation in simulated body fluid (SBF). Also the biological studies such as direct contact test, MTT assay, Alamar blue test and Cell adhesion revealed the cell friendly nature of the surface coating.

Unlike the other reactions of titanium surface modification, the hydrothermal reaction can be easily controlled by the alteration of precursor concentration. Also this technique can be used for surface-modifying implants of any shape so that a bioactive and osseo-integrating surface is created.

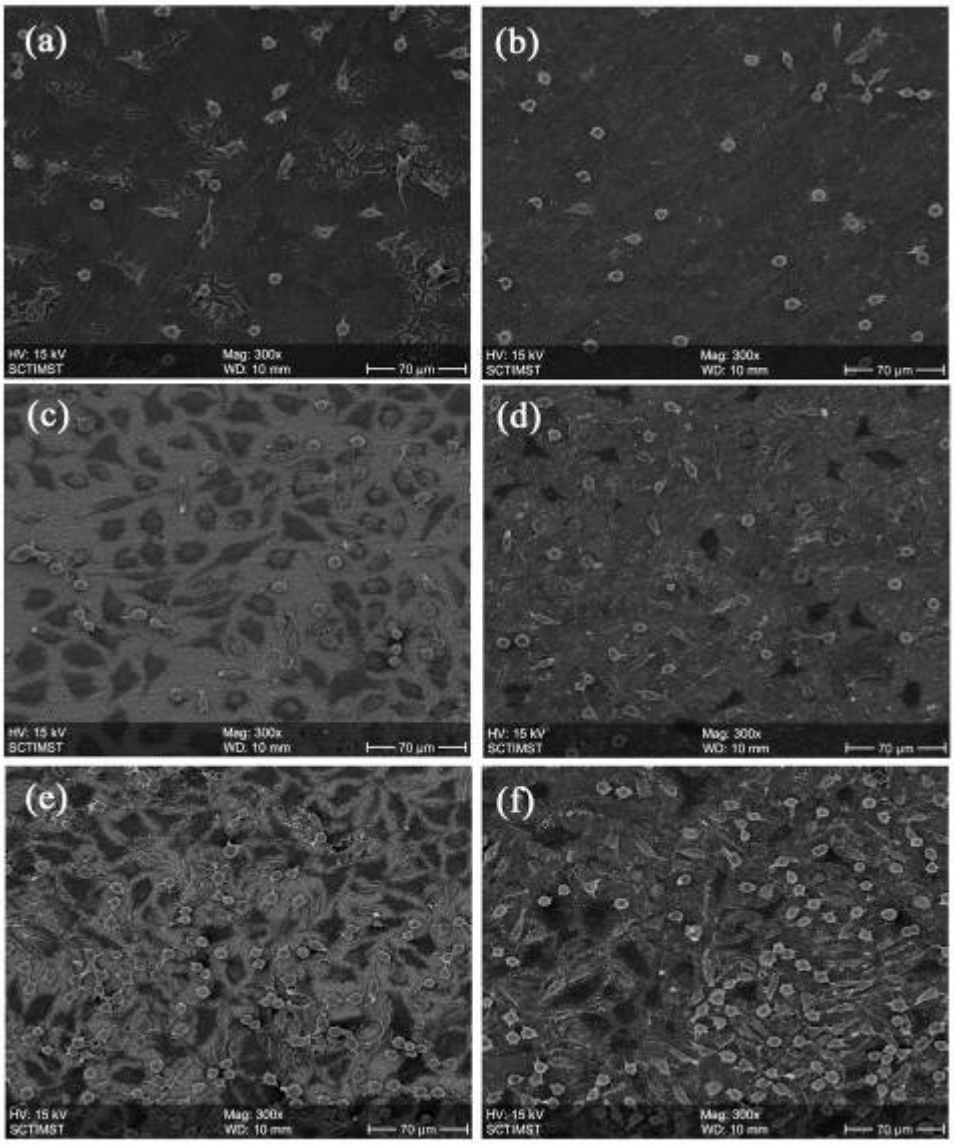

Figure 28. The SEM micrograph of the cell seeded surface of Ti (left) and Ti HT (right), (a,b - 24h), (c,d - 48h), (e,f - 72h) respectively.

5. IMPLANT DEVELOPMENT AND COATING

5.1 The new dental implant design

A complete dental implant system, with screw and abutment, has been developed by the team in IISc, Bangalore. The screw part of the implant system was made tapered to reduce the resistance in bone while implantation. The abutment part has a modified fitting for better stability. The design verification has been done by an expert team. The schematic of the implant system is shown in Figure 29.

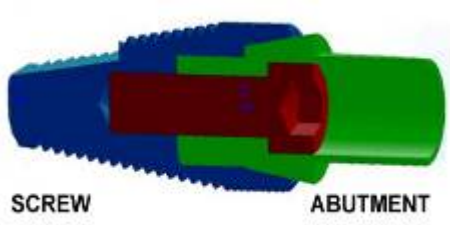

Figure 29. Schematic of the design of the new dental implant system

The newly designed dental implants were fabricated by special machining, out of imported certified batches of Ti-6Al-4V. Hybrid machining modality with computer numerical control (CNC) machining and electrical discharge machining (EDM), has been adopted. The implant screw part was shaped into the conical / tapered screw of with 5.0 mm diameter at the upper threaded end and 3 mm at the lower threaded end, terminating with a dome of 2.5 mm radius.

Micro V-threads were given on the collar region having 0.35 mm pitch and 0.2 mm height. The apical or tapered portion of the implant is characterized by buttress threads having 0.5 mm and 0.3 mm respectively, with 45° alignment. The test implant contains 3 mm long straight healing chamber. The primary purpose of the healing chamber is to collect bone chips and blood during the implant insertion. A major portion of the healing and process of osseointegration starts with the healing chamber. Sandblasting and acid-etching (SLA) technique are used for modifying the surface of implant screw to reduce the healing period between surgery and prosthesis.

5.2. Implants surface modification using HA coating via PLD technique

The coating of hydroxyapatite was made on the screw part of the newly fabricated implant system, in PLD system at optimised conditions. The screw part was scrubbed in soap to remove dirt and grease and ultrasonically cleaned in de-ionized water, ethanol and in acetone. It was then mounted vertically in the system on a rotating spindle at 4cm from the target and heated up to 400^{o}C. The target was ablated with 355nm laser at a repetition rate of 10 Hz and a power of 2 W, focused to 2 mm spot size. The deposition was done for 60 minutes, to obtain a coating of about 4microns thickness. It was then subjected to SEM analysis, including EDS to look into the composition.

The results of the SEM-EDS analysis are represented in Figure 30. The HA coating on the threads of the screw was remarkably uniform, with microstructure as noticed in the case of flat samples. The Ca/P ratio calculated from the EDS data is 1.69, close to the theoretical ratio of hydroxyapatite.

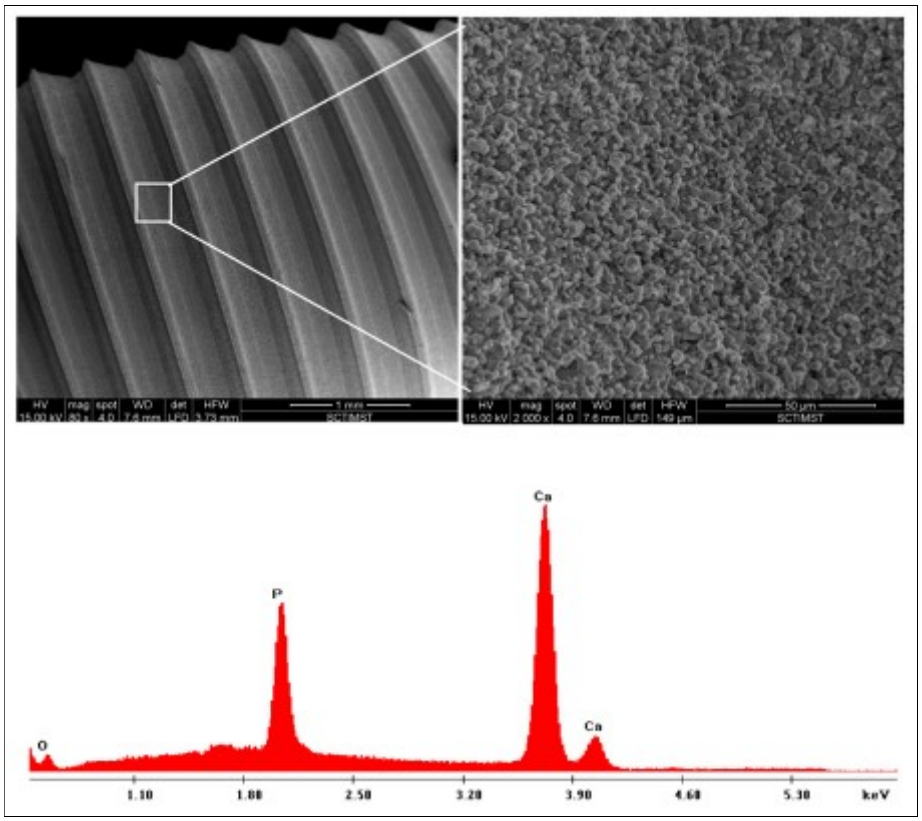

Figure 30. SEM of HA coated over dental implant (screw) using PLD technique, and the EDS spectrum showing the Ca/P ratio.

6. ANIMAL IMPLANTATION

6.1 The rationale and plan of animal implantation

Any new biomaterial developed for implantable device should undergo implantable tests in animals to prove its safety and functionality. In the present case, animal implantation experiment is planned to verify the local bone response to the implant, placed in an appropriate bone defect as per an accepted procedure. Both the responses to implant material as well as the design were to be looked into. Rabbit femoral condylar implantation model was selected for the reasons of more convenience and lower cost. The International Standard ISO 10993 prescribed for biocompatibility of materials, support rabbit bone implantation as an agreeable test.

The selected experiment involves the implantation of the screw part in the femoral condyle of rabbits. The newly designed implant will be compared with a standard commercial implant. The implantation period will be so selected that the major healing or remodeling events are covered. On the completion of the period, the implants along with the surrounding tissues, will be excised for histological and micro-radiographic examination. In addition, for research interest, it is planned to explore the expression of osteogenic genes in the implanted site. It will give an idea of the bone regeneration capacity.

The implantation experiments are intended to be conducted in SCTIMST animal facility, after satisfying all the ethical stipulations. The animal care and implantation procedures were done as per accepted International Standards.

6.2 Implants for animal experiments

The new implant system with tapered screw profile of 4 mm diameter and 6 mm length was used for implantation experiments. ‘Straumann’ brand commercial implant (cylindrical design) with maximum diameter of 5 mm and maximum length of 6 mm, was selected as control. The Ti6Al4V based 6 mm long Straumann® Titanium SLA® dental implant is used as the control material for this study. It has two V-threads on its external surface and the shape of the implant is almost cylindrical ended with a dome. Additionally, it has bone anchorage surface, which was modified by sand blasting of large particles and subsequently etched, commercially known as SLA technology. The pictures of the implants along with the photos are given in Figure 31.

6.3 Animal selection :

The aim of the animal experiment is to verify the local bone response to the implant, placed in an appropriate bone defect as per an accepted procedure. According to the International Standard ISO 10993, this kind of a study could be done reliably in a rabbit model. Rabbits, in general, react similarly to humans to diseases and medications.

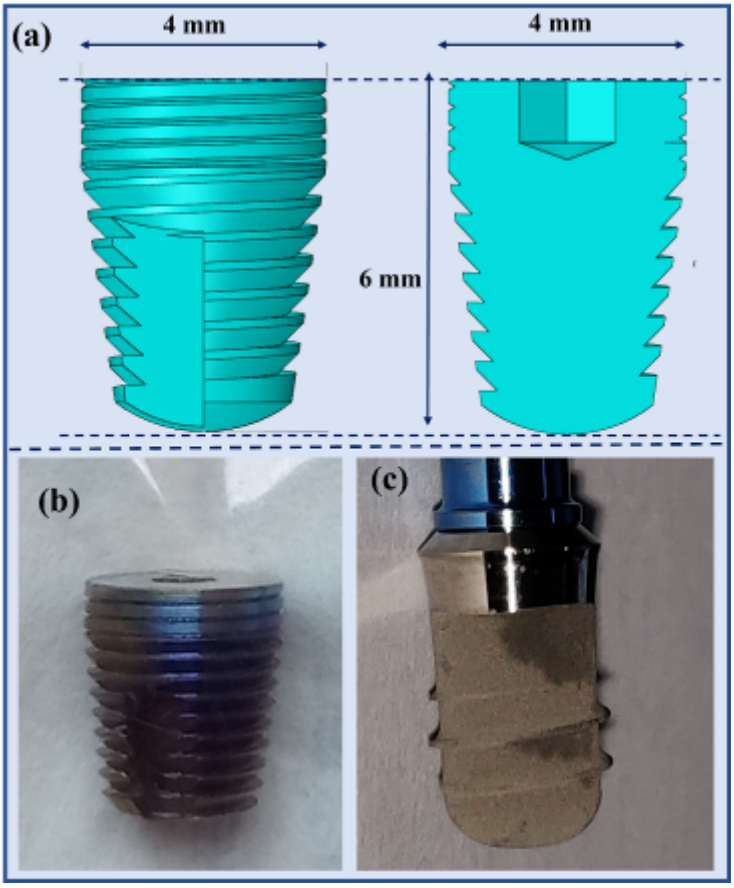

Figure 31: (a) The 3D CAD model of the Ti6Al4V based test implant and cross-section of the hybrid threaded tapered implant. The cylindrical collar portion of the implant contains micro V-threads and the tapered body contains buttress thread. Macro photographic images of (b) as-machined hybrid threaded tapered test implant and (c) Straumann® Titanium SLA®, the control implant.

White colored New Zealand rabbit breed was selected for the test. New Zealand rabbits are a common choice for laboratory testing because of their docility and good health. Their femoral bones have space in the codyles to accommodate implants of 5-6 mm size.

This study will be done in two parts – (i) Essential biocompatibility study as per ISO 10993, in which the samples are implanted in rabbit bone and healing/remodeling pattern is observed; and, (ii) Gene expression study, in which the bone regeneration capacity is assessed by identifying the expression of osteogenic genes. In the biocompatibility study, 10 implants are to be tested in the test group as well as in the control group. In a single animal, one test and one control could be implanted in the left and right femurs. Therefore, the essential biocompatibility study could be done in 10 animals. Similarly, 8 animals are needed for implantation to conduct the gene expression study. The animal requirement for the complete activity is 18.

In-house bred animals of 12-24 months age, of either sex were kept ready for the study. At that age, they will gain a weight in the range 2500 - 3500 gms. The duration of implantation is decided to be 12 weeks. At that period, the remodeling of the defect site will be clearly observable.

The animal study plan was submitted to the Institutional Animal Ethics Committee (IEC) and approval was obtained by (B form number: SCT/ABS/IAEC/96/1). The implantation protocol was based on the ISO 10993-6 standards.

6.4 Animal care

The animal care was done following the ISO 10993-2 Guidelines and CPCSEA Guidelines. The animals were caged in standard stainless steel cages with food hopper and water sipper. The cages were laid with husk bed with tray change daily and full cage cleaning twice weekly. Clean sterile food was given to the animals *ad libitum*.

The cages were housed in a room maintained at temperature of 22±2°C and humidity 30-70%. The room had HEPA filtered air, with air change frequency of 12 times/hr. The light cycle was 12h Day-Night. The animals were acclimatized for 15 days before surgery.

6.5 Implantation procedures

This study was aimed to evaluate the local effects and bone formation around implant *in vivo* in rabbit femur. The procedures were done in an operation theater having all the essential facilities, by a trained veterinary surgeon and a consultant dental surgeon (Figure 32a).

Figure 32. Surgery preparations - (a) The surgery set up; (b) Site preparation in the animal, and (c) Making the incision.

6.5.1 Preparations

The animals (rabbits) were anaesthetized with a combination of Atropine at the rate of 0.25mg/kg BW, Xylazine at the rate of 5mg/kg BW, and Ketamine at the rate of 50mg/kg BW. Anaesthesia was maintained by 1.5% isofluorane through face mask. The lateral sides of the thighs were prepared aseptically (Figure 32b and 32c). A linear skin incision was made on the medial aspect of the stifle joint and the muscles were retracted to expose the distal aspect of the femur. The periosteum was retracted to place the implant, in the drilled holes. The test implant was placed on the left limb and the control implant, on the right limb.

6.5.2 Implant placement

The implantation was done using the tool kit associated with the implant. Drillings were made under saline irrigation using a low speed dental drill, to a depth of 6mm.The defect creation was started with pin drill tool followed by pilot drill of 2mm diameter. The diameter of the defect was increased stage by stage to 5mm using osteotomy drill.

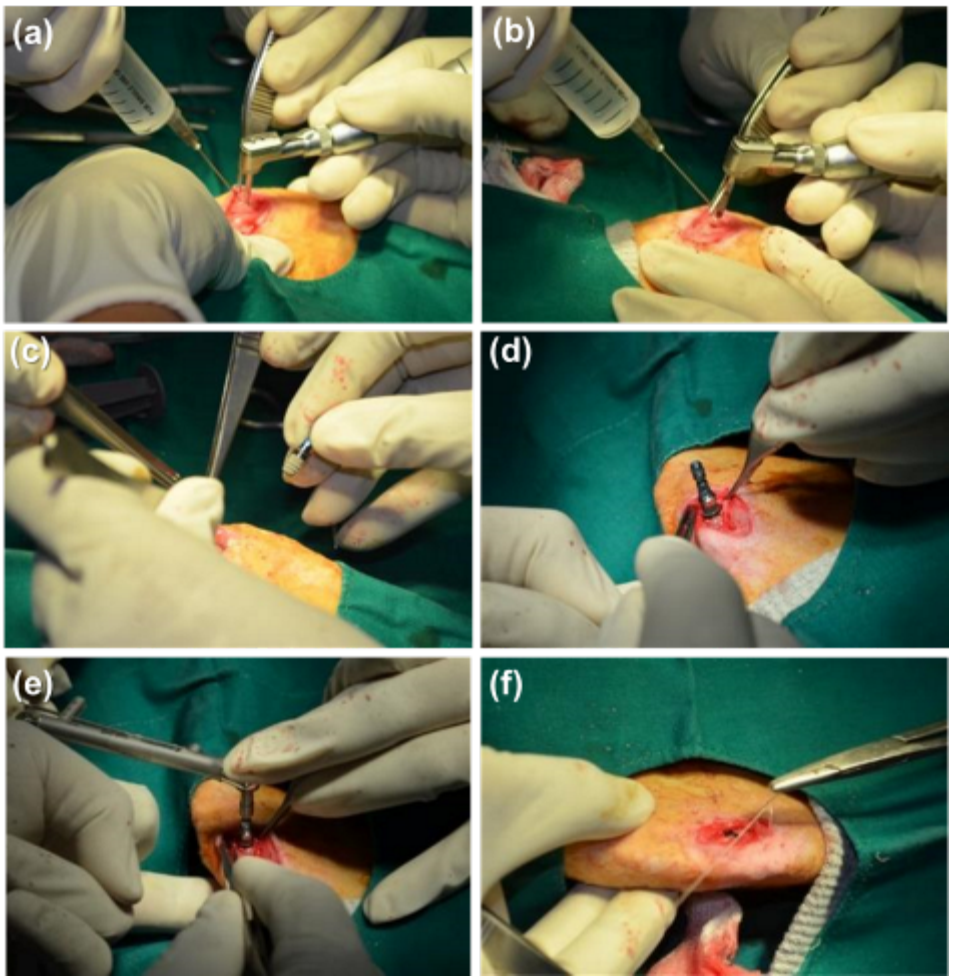

Figure 33. The various steps during the implantation – (a) Pilot drilling ; (b) Expanding with osteotomy drill ; (c) The implant placement in the drilled hole ; (d) Adapter fitted for tightening; (e) Final tightening using ratchet ; and (f) Suturing the wound.

The test and the control implants were placed and threaded into the defect with the help of a torque controlled ratchet. The various steps of the surgery are shown in Figure 33.

6.5.3 Post-operative care and explantation

On finishing the implantation, the retracted muscles were released and replaced. The cut subcutaneous fat and superficial fascia were sutured in the first tier and the skin incision was closed in the second tier. Post-operatively, the wound was dressed routinely and all the animals were put under antibiotic coverage with analgesics for the immediate seven days. Standard animal care was given to all the experimental animals till the end of the period.

The animals were sacrificed 12 weeks after implantation and femur bone with the implants were retrieved for histological evaluation. Implant interface bone tissue, as well as normal bone tissue, were collected for molecular studies and stored in a falcon tube containing RNA*later*™ (Thermo Fischer, USA). For histological studies, the collected bone tissue samples were fixed and stored in 10% neutral buffered formalin (NBF).

7. OUTCOMES OF THE *IN VIVO* STUDIES

The previous chapter described the animal implantation procedures, which is ia crucial step towards investigating the biological response of the newly developed implant. The study is so planned that both the influence of the material as well as the shape/design of the implant to the surrounding tissues will be revealed in the further analysis. This chapter describes the various analyses of the implanted samples staged, like Histopathology Analysis, Bone Histomorphometry, Micro-CT Analysis, and Gene Expression Studies. The methods and results are discussed in various sections below.

7.1 Studies on implanted samples

7.1.1 Histopathology

This part involves the microscopic observation of the histological sections of implanted area to identify the bone growth features around the sample.

Cross-sectional blocks of bone having both control and test implants, were cut using low speed precision saw. Further, cross-sectional blocks were again fixed with 10% NBF and followed by dehydration in ascending grades of alcohol (70%, 80%, 96% and 100%). The dehydrated tissue blocks were embedded in Poly Methyl Methacrylate (PMMA). A number of thin sections (150-180 µm) of implants with surrounding bone embedded in PMMA resin were sectioned using high-speed precision saw microtome (Accutom 100, Denmark). For clear microscopic vision, tissue sections were further ground and polished using a grinder polisher machine (ECOMET 3000, Buehler, USA). Resin embedded thin sections were then stained using Stevenel's blue stain in the pre-heated water bath for 5 minutes. The excess stain was removed by dipping in distilled water in a boiling water bath. These resin sections were then counter-stained with Van Gieson's Picro-Fuschin stain for 3 minutes at room temperature. The excess stain was removed. Stained sections mounted on glass slides were viewed under a bright field trinocular microscope (Nikon NiE, Japan) and microphotographs were captured using the attached digital camera (Nikon DS-Ri1).

7.1.2 Histomorphometry

The area percentage of the neobone formed in peri-implant space between the implant and host bone could be determined by Histomorphometry. It is performed by analysing the multiple sections taken from the peri-implant or proximal site of the implant after 12 weeks of implantation. The photomicrographs of bone with implant were analysed and the quantification of the neobone was carried out by using the Image J software (U. S. National Institutes of Health, Bethesda, Maryland, USA). The percentage of the total length of bone contact with the implant to the total length of the implant was calculated as, BIC:

$$\text{BIC \%} = \frac{\text{Total length of bone contact with implant}}{\text{Total length of implant}} \text{ X } 100$$

Bone to implant contact percentage (BIC) was calculated for both test and control implant sites by selecting the region of interest using multiple selection tools of the software. This method using Image J is considered as the standard technique used to quantify the information about the microscopic structure.

7.1.2 Micro-CT analysis

Micro-CT analysis was carried out to analyse the mineralization of neobone formed around the control and test implants after 12 weeks of implantation. It also helps in analysing the newly formed bone morphology and to quantifying neobone with respect to the host bone. These analyses were carried out using high-resolution X-Ray micro-computed tomography (µCT40, Scanco Medical, Switzerland). Retrieved bone samples along with implants were first fixed with 10% NBF.

The scanning of the samples were carried out with X-ray tube settings, at voltage 70 kV, and filament current 57 µA, and voxel size of 20 µm. The exposure time was approximately 300 ms for the image acquisition of each slice. The specific area of implant and neobone was selected and reconstructed using the cone beam convergence algorithm of the software provided with the equipment. 3D reconstructed images of sample/bone can be obtained using micro-CT, by rotating micro focal X-ray projections through multiple directions. Based on density alteration, three-dimensional (3D) images of the bone and implant were acquired, based on the distinction between the region of interest (ROI) and volume of interest (VOI). After thresholding, the bone volume (BV) was determined by counting the total number of bone voxels and multiplying by their known volume, while the total volume (TV) was determined by counting the bone and non-bone voxels. Bone volume (BV) to total volume (TV) ratio, also known as bone volume fraction (BV/TV), was determined after thresholding and segmentation and bone mineral density (BMD) was measured.

A series of about 302 slices in 2D with a scanning resolution of 6 µm were obtained by irradiating the specimen with penetrative X-rays of 45 keV. µ-CT Tomography V5.5 software was used as image processing and µ CT Evaluation Programme V6.0 was used for evaluation. The apposition of the host bone with the implants, and bone density were evaluated by 2D histomorphometric analysis at a threshold Th 27.

7.1.3 Gene Expression Studies

(i) Total RNA extraction and cDNA synthesis

The implants, both the control and the test, and the attached peri-implant host bone of four rabbits were carefully collected using trephine at the end of the 12 weeks. Collected bone samples were washed using Diethyl pyro-carbonate (DEPC) treated water. Bone tissue specimens were kept in RNA*later*™ (Thermo Fischer, USA) and stored in minus 70˚C until analysis.

Total intracellular RNA was extracted according to the protocol provided by the TRIzol^{R} (Invitrogen). The bone tissue sample was taken out from RNA*later*^{TM} and thawed at room temperature, followed by washing using DEPC treated water. The washed samples were then crushed using mortar and pestle by adding liquid nitrogen while kept in cold dry ice. The crushed bone samples were homogenized using tissue homogenizer (Polytron, Kinematica Inc.). The phase separation of DNA, RNA, organic components and proteins was carried out by adding chloroform. The content mixed with chloroform was centrifuged at 12000rpm for 15min at 4˚C. The colorless liquid top layer had RNA, and semisolid middle layers contained primarily DNA and red colored bottom layer contained organic solvents and proteins. RNA was carefully collected and precipitated by adding isopropanol and centrifuging the mixture at 12000rpm at 4˚C for 10min. The precipitate of RNA was cleaned using 75% ethanol. The RNA purity and quantity of isolated total RNA were checked at OD 260/280 nm and quantified at OD 260 nm by using a Nanodrop spectrophotometer (Nano Drop Inc. Wilmington, USA).

Transcriptase core kit (RT-RTCK-03, Eurogentec, Belgium) was used for cDNA synthesis and the kit protocol was followed for cDNA synthesis from isolated mRNA samples. Reverse Transcription (RT) was performed with 10 µL reaction mixture for each sample, which contained 1 µL 10X buffer solution, 2 µL of 25 mM $MgCl_2$, 2 µL of 2.5 mM dNTPs (dATP, dCTP, dGTP, dTTP), 0.5 µL oligo d(T) 15VN, 0.2 µL RNase inhibitor, 0.25 µL Euro Script RT, and 200 ng RNA template. The solution was made up to the desired amount by adding RNase free water. Prior to the mixing, all the reagents were thawed. For polymerase chain reaction (PCR) of cDNA synthesis, the reaction mixture was pre-heated in the Thermal cycler (Eppendorf, USA) for 10 min at 105˚C. The reaction mixture was annealed at 25 ˚C for 5 min and extended at 42 ˚C for 1 hour. The cDNA samples were stored at -20 ˚C until further use.

(ii) Gene expression using RT-PCR

Real-time Quantitative Reverse Transcription (RT-PCR) was performed with a 20 µL RT-PCR master mix with custom-designed primers. Forward and reverse primers of the genes to be analysed were designed using BLAST and are mentioned in **Table 1**. Takyon™ No Rox SYBR® Master Mix was used for the gene expression study following the kit protocol using the Real-Time thermal cycler qTOWER 3 (Analytik Jena, Germany). Amplification, quantification, and gene expression of COL1A1 (Collagen type I alpha 1), SPP1 (Secreted phosphoprotein 1), SPARC (secreted protein acidic and rich in cysteine), RUNX2 (Runt-related transcription factor 2), VEGF (Vascular endothelial growth factor), and GAPDH (Glyceraldehyde 3-phosphate dehydrogenase) was analysed in this study. 2.5µL of cDNA template was transferred into a clear thermo-fast 96 well plate (Axygen, Denmark) with reaction mix containing 1.2 µL of forward and reverse primer mix, 10 µL of Takyon™ No Rox SYBR® Master Mix and to a total volume of 20µL with nuclease-free water. The plate in the thermocycler was run for enzyme inactivation at 95˚C for 3min followed by denaturation at 95 ˚C for 3sec; annealing at 60˚C for 20sec and extension at 72˚C for 30sec.

Table 1: Forward and reverse primer sequences used for Real-Time RT-PCR

Sequence	***Oligoname***	***5'----------3' Sequence***	***Base pairs length***
1	Collagen 1 forward	GCAAGAACGGAGATGACGGA	20
	Collagen 1 reverse	TTGGCACCATCCAAACCACT	20
2	RUNX 2 forward	ACCAGTCTTACCCCTCTTACCT	22
	RUNX 2 reverse	AGGTGCTGGGCTCTGAATCTG	21
3	SPARC forward	GAAGTAGTGGCCGAAAACCC	20
	SPARC reverse	TGGGGGTGTTGTTCTCATCC	20
4	GAPDH forward	CAACGAATTTGGCTACAGCA	20
	GAPDH reverse	AAACTGTGAAGAGGGGCAGA	20
5	VEGF forward	*CTTGCAGATGTGACAAGCCG*	20
	VEGF reverse	*AGTCTTTCCCGGTGAGAGGT*	20
6	SPP 1 forward	CGATGACTCTCACCACTCCG	20
	SPP 1 reverse	CTGCGAAATTCACGGCTCTG	20

(iii) Data analysis

The cDNA copy number of the target gene was normalized with the reference gene, GAPDH (housekeeping gene). Real-time PCR data was converted to delta C_t value and then relative gene expression was calculated using delta-delta C_t method ($\Delta\Delta C_t$) as per the given equation

$$\Delta C_t = C_t \text{ of target gene} - C_t \text{ of reference gene}$$

$$\Delta\Delta C_t = \Delta C_t \text{ of test sample} - \Delta C_t \text{ of control sample}$$

The fold change, also known as relative quantification, is defined as $2^{-\Delta\Delta C_t}$. The relative quantification was used to assess the fold change in gene expression over time. The level of specific mRNA of the genes of interest was calculated by subtracting the C_t value of the reference gene (GAPDH) from the gene of interest. The control group was used as a reference and normalized with the test group in the calculations.

7.2 Results

7.2.1 Gross observations of the implanted area

The control and test implants placed in the medial femoral condyle during the surgery is shown in Figure 34 (a) and (b), as recorded before closing the wound.

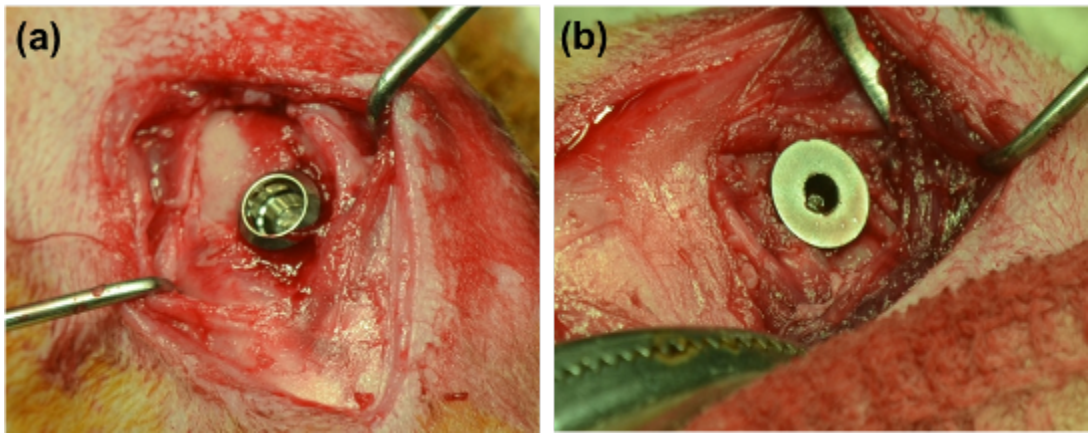

Figure 34. View of the implanted site (medial femoral condyle) immediately after implantation (a) The control implant (b) The test implant.

The test and control implanted femurs were collected in 10% buffered formalin by autopsy and transferred for grossing examination by histopathologist. The implant sites were identified after clearing the bone surface. The gross view of the implanted sites (test and control, corresponding to those in Figure 34) could be found in Figure 35(a) and (b).

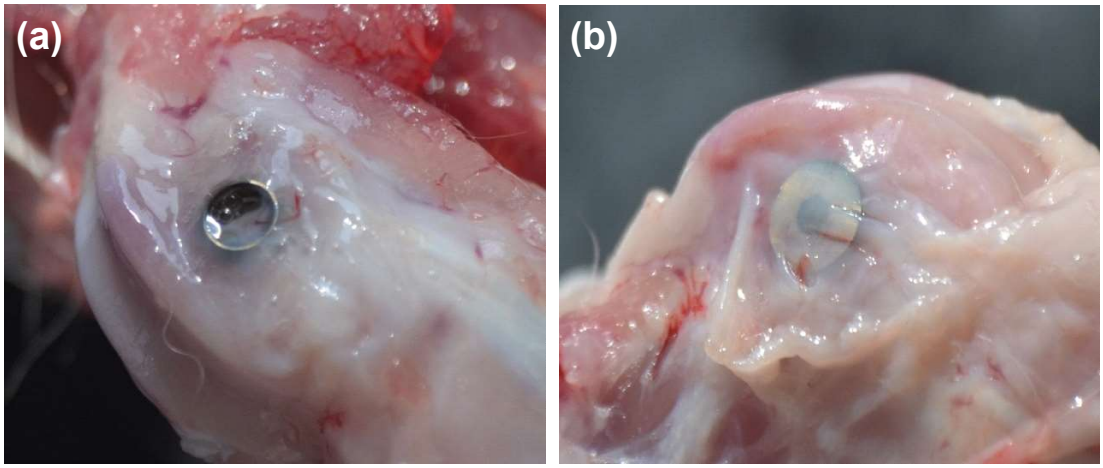

Figure 35. Gross image of the retrieved implanted medial femoral condyle after 12 weeks (a) The control implant (b) The test implant

7.2.2 Micro-CT analysis

In the present study, the micro-CT results are analysed quantitatively and qualitatively to assess the mineralization and morphology of neobone formed around both control and test implants (Figure 36). It is quite evident from the images that both implants were in physical contact with the neighbouring neobone.

The 3D morphology of bone formed around implant interface after 12 weeks of implantation revealed a high ratio of bone volume fraction (BV/TV = 0.46) in the case of test implant, and a significantly low bone volume fraction (BV/TV = 0.16) in the case of control implant (Figure 36, a1 and b1). Cross-sectional micro-CT tomograph showed that better integration of test implants with host bone and better trabecular construction and more organized supporting bone around it than control implant. Two dimensional (2D) tomographs of central slice showing the micro-architecture of the neo-trabecular bone and host bone around the control and test implant (Figure 36, a2 and b2).

After 12 weeks of healing, the bone mineralization (BMD) of neobone around the test implant showed marginally lesser values when compared to the control. In the case of control, BMD was observed to be 1583 mg HA/ccm, whereas, in the case of test implant, it was found to be 1425 mg HA/ccm. But micro-CT images showed better trabecular support and neobone formation around the test implant.

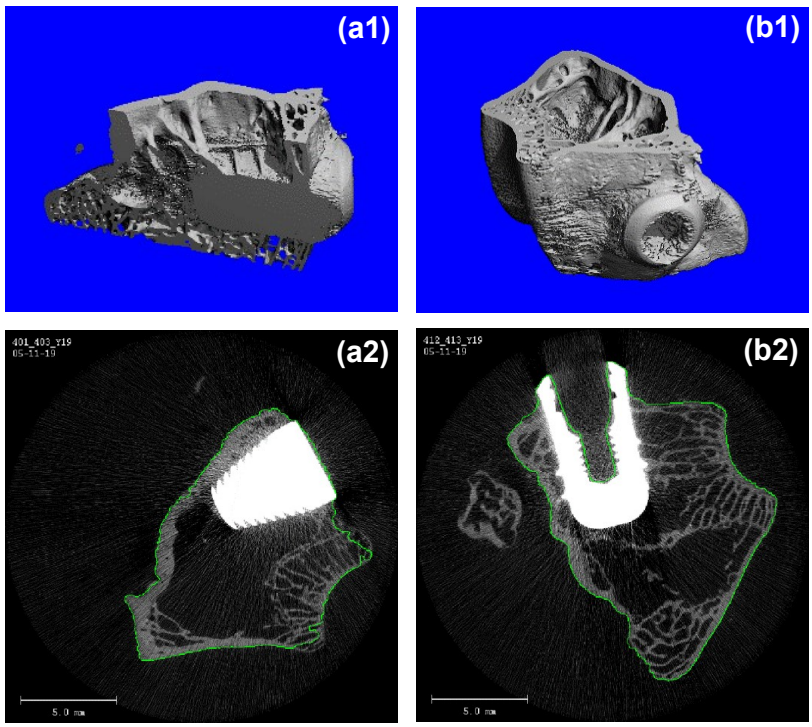

Figure 36. The Micro-CT results of the retrieved implant in bone. The top images a1 and b1 show the 3D constructed image and the bottom images a2 and b2, the 2D middle slices. The left side images (with the prefix 'a') correspond to test implant and the right side images (with the prefix 'b') correspond to control implant.

From the 2D histomorphometric analysis in microCT, it could be seen that the surrounding bone is intact without any osteolysis, or local damage. Apparently, good bone apposition was seen and the implants were stable.

7.2.3 Histological observation

The sections of implanted sites were subjected to microscopic evaluation. No evidences were seen for necrosis, inflammation or degeneration at the implant-bone interface (Figure 35). Any intervening soft tissue between the implant and bone was not observed.

The gross histologic observation presented clear signature of bright yellow color stained neobone formation at the end of 12 weeks, around both test and control implants (Figure 37).

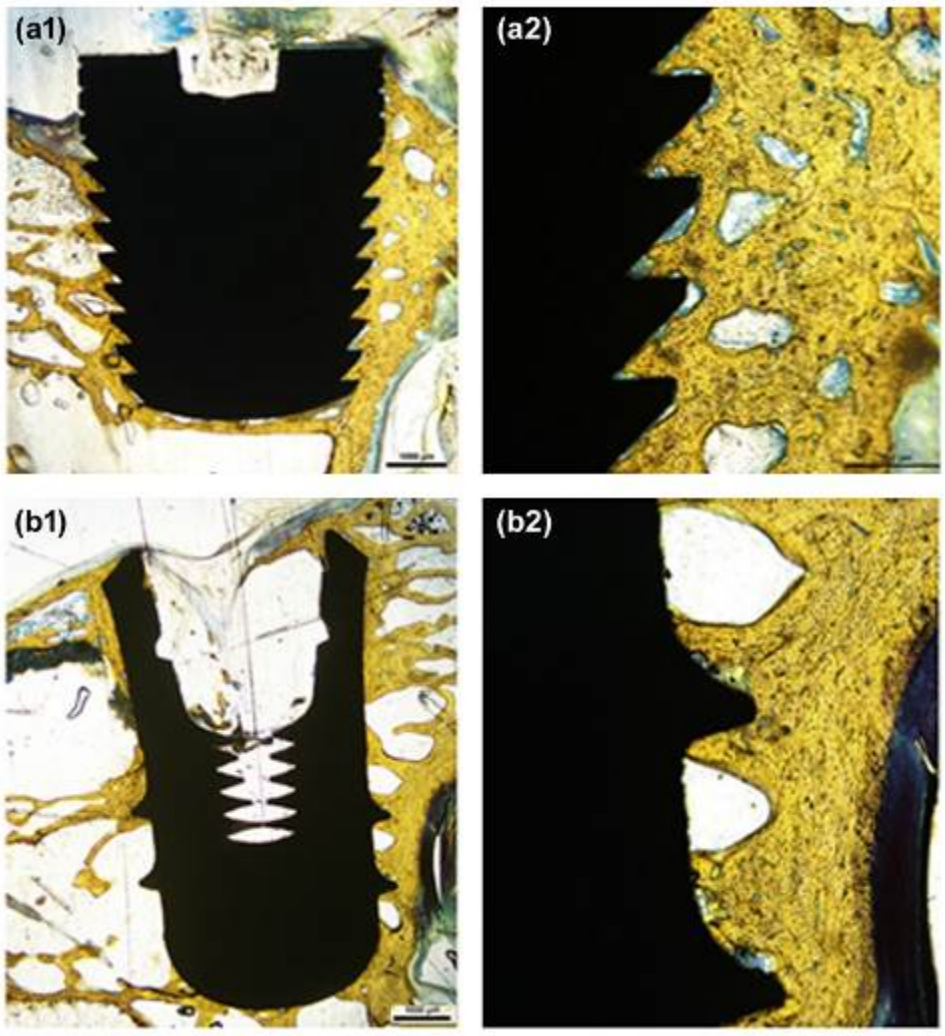

Figure 37. The histological results of the implanted screws in bone, after 12 weeks. Image set 'a' corresponds to test implant and 'b' corresponds to control implant. Full image of the implant is shown in the left image set (a1 and b1) and the corresponding implant-bone interfaces on the right (a2 and b2). Bone is stained yellow.

Implants were observed without any gross abnormalities like budging, fluids collection or breaks in the implant-bone interface. Osteoblast activity was observed in both test and control implants. Histologically, no qualitative difference in the neobone formation could be noted between control (SLA) and test implants.

In the sections of the test site, new woven bone and lamellar bone were observed following the thread morphology of both micro-V threads and buttress threads and hence filling the complete interface of the test implant, even in the marrow region of the condyle (Figure 37, a1 & a2). In comparison to the test implant surface, the control implant revealed multiple areas of implant surface not covered with neobone (Figure 37, b1 & b2). Around the collar region of the control implant, a dense cortical bone was observed. But in the marrow region, neobone formation was discontinuous and did not cover the whole entire implant surface.

Multiple foci of neobone formation with rosettes of osteoblasts were noted at the interface of both control and test implants. Similar pattern was seen in the grooves of the test implant. Mature new woven bone and lamellar bone were observed with well-developed 'Haversian system' or 'osteons' along the test implant thread geometry.

7.2.4 Histomorphometry

The maximum bone-implant contact after 12 weeks of implantation was observed in as-machined test implant (Ti6Al4V material), compared to SLA treated control implant (Titanium). The control implant has shown 67.85% of neobone formation or surface apposition at the bone-implant interface, whereas the test implant has shown 78.65% of neobone formation (Figure 38). The quantitative analysis of new woven bone formation across the implant interface showed an enhanced neobone formation in the test group, when compared with the control group with a significant difference.

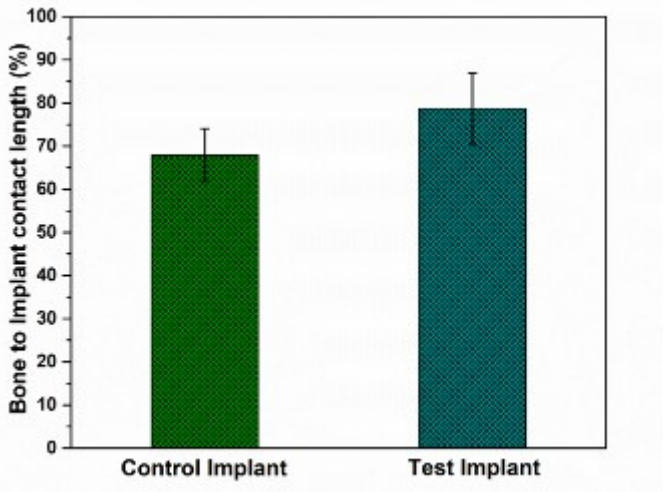

Figure 38. Graphical representation of contact percentage of neobone formation estimated from the region of interest between the implant and host bone interface in rabbit condyle after 12 weeks. Error bar indicates ± standard deviation (n = 4).

7.2.5 Gene expression pattern

The expression of osseogenic genes (COL1A1, RUNX2, SPARC and SPP1) and Angiogenic gene (VEGF) were quantitatively determined using RT-PCR, and fold change was recorded. GAPDH gene was used as the reference gene. Gene expression of test and control samples was normalized with the normal bone sample (figure 39). The expression of COL1A1, RUNX2 and SPARC genes were found to be up regulated in acid etched Ti implant. The osteopontin, SPP1 was found to be down regulated. The up regulated expression of COL1A1, RUNX2, and SPARC indicates that the bone was under mineralization phase. The main structural protein, COL1A1 was the major component in organic phase in bone. They actively participated in the bone mineralization phase. Bai et al., 2020 has reported that the COL1A1 gene expression increased while studying biomimentic osteogenic peptides in chronic inflammatory patients. The COL1A1 expression along with other genes indicated osseogenesis. RUNX2 gene transfer study in MSCs had identified that the Runx2 gene has osseogenic activity and the osseogenic activity has been enhanced by the adenoviral transfer of RUNX2 gene in MSCs (Zhao et al., 2005). Delany and Hankenson in 2009 studied the gene expression of SPARC in the bone mineralization and proliferation, SPARC gene expression revealed the role of SPARC in the bone remodelling process. They have shown a wider pattern of activity in both mineralized and non-mineralized tissue (Rosset and Bradshaw, 2016).

SPP1 gene found to be down regulated in both control and test, and expressed in normal tissue (figure 39). The SPP1 down regulation in tissue with surface treated implants is indicating that the bone is under mineralization. Osteopontin is a non-collagenous protein present in the organic phase of bone mainly in the mineralized bone matrix. The high expression of SPP1 in normal bone is due to the mineralized bone matrix in normal bone compared to the surface treated implants. SPP1 has a role in bone metabolism and they are mainly seen in the mineralized tissue. A bone niche recapitulation study on rabbit model conducted by Minardi et al., in 2019 observed the SPP1 gene expression in mineralized bone along with other osteogenic markers. Foster et al.,2018, had studied osteopontin's (SPP1) effect on dental mineralization and they reported that the SPP1 has been expressed in the mineralized bone in early osteoblasts during periodontal tissue formation (Foster et al., 2018).

The expression of VEGF was found to be up regulated in acid etched Ti implant (figure 40). VEGF promotes the new blood vessel formation in and around the newly formed bone. VEGF has a major role in coupling angiogenesis and osseogenesis. Izquierdo-Barba et al, in 2019 studied the effect of VEGF absorbed Ti scaffold in osteoporotic sheep. It has been observed that the VEGF scaffold had promoted the angiogenesis and had shown an improved effect on ossification.

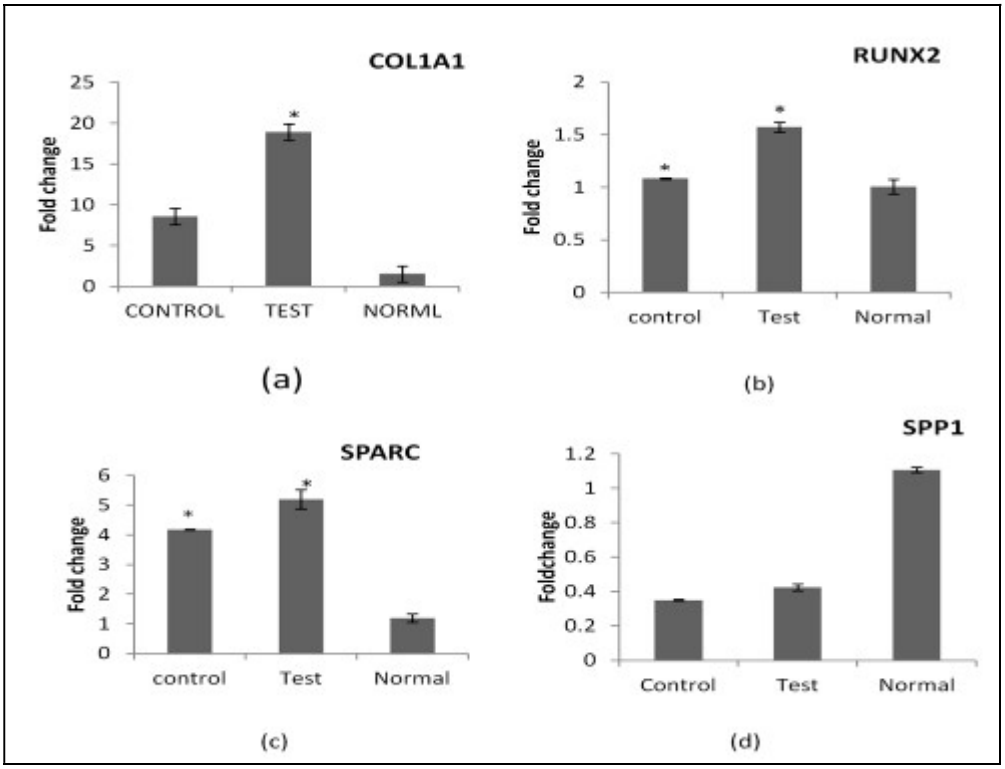

Figure 39. Graphical representation of RT-PCR data - COL1A1, RUNX2, SPARC and SPP1, depicting the fold change in expression values, Mean±SD (n=3). P value <0.05 (significant value compared with non grouped normal bone); (a) COL1A1 (b)RUNX2 (c) SPARC (d)SPP1 (*Abbreviations : COL1A1- Collagen type I alpha 1,RUNX2-Runt-related transcription factor 2, SPARC- secreted protein acidic and rich in cysteine,SPP1-Secreted phosphoprotein 1)*

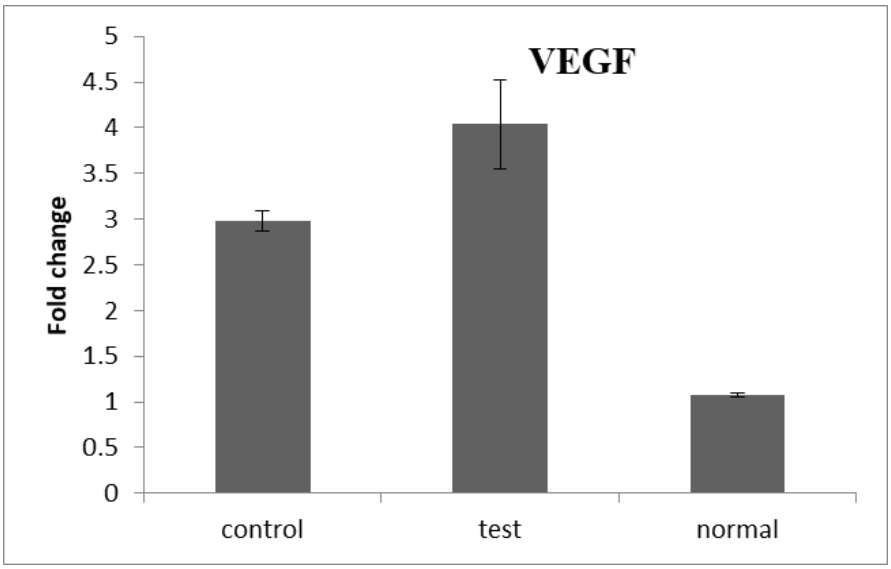

Figure 40 : Graphical representation of RT-PCR data- VEGF, depicting the fold change in expression of VEGF gene (values are represented in Mean ±SD (n=3). P value <0.05, *(Abbreviation: VEGF-Vascular endothelial growth factor)*.

7.3 Discussion and Remarks on the in vivo experiments

This animal study on osseointegration study is carried out to assess the effect of implant design and thread geometry on the quality of osseointegration and primary stability. It is known that the geometry of the threads and implant shape determines the surface area available for stress transfer and governs the initial stability of the implant. The rationale behind adding micro-threads on the collar portion of the test implant was that it would improve the primary stability and lead to better stress distribution in the crestal region of the bone. Also, it is assumed that a large number of threads and micro-threads would provide more surface area for bone apposition on the implant surface and, as a result, early osseointegration will take place.

7.3.1 Early osseointegration of hybrid threaded dental implant and contact guidance mechanism

Over 12 weeks of implantation no experimental animals showed any observable complication post-operatively. Nevertheless, the histological observation does indicate the difference in the overall healing pattern in terms of the growth and the amount of neobone formation between test and control implants. In gene expression studies also, the upregulated biological response and higher bone volume were observed in the case of test implant in comparison with the control implant.

It was seen that the neobone is covering the entire test implant surface and filling all groves without any discontinuities, even in the marrow region of the condyle. Osteoblasts were also observed towards the underlying layer at the implant surface. Whereas, in the case of control implant, woven bone was found to be discontinuous and not covering the complete available surface, despite having micro pits and cavities which usually promote osseointegration. In histomorphometric observations, 78.65% of bone to implant contact (BIC) was measured in the case of the test implant and 67.85% of BIC in the case of the control implant. Therefore, it can be said that in the newly developed hybrid threaded test implant, the available area for bone apposition was more. Also, the threads were able to distribute the load in such a manner that neobone formation and bone remodeling can be triggered. In the control implant, the available macro surface area was less, but the availability micro surface area was sufficient as it was SLA surface-modified, and bone apposition was observed to a lower extent on the implant surface.

The reason behind more bone apposition on the test implant can be that micro-V threads on the collar region have relieved excessive stress concentration, giving an optimal stress that might have stimulated neobone formation. It could be ascertained that the geometry and number of threads help in bone remodeling. Also, the healing chamber of the test implant might have also influenced the biological bone healing sequence, compared to traditional cylindrical screw shaped implant without any healing chamber. Formation of blood clots during implantation in the chamber can provide cues for healing.

One of the possible reasons behind better osseointegration on implant surface could be the contact guidance of the bone cells with the threads available on the surface as substrate, i.e. cell migration in a direction. Contact guidance is the ability of the bone cells to sense and align with the anisotropy of the surrounding micro-environment. The grooved topography is thought to stimulate cell migration and induce guided contact osteogenesis. The extent of such a phenomenon is dependent on the dimensions of the groove. Hall et al. proved that the geometric grooves, which are clearly larger than osteoblasts, stimulate directed bone growth and deposition within the grooves, consequently optimizing implant stability.

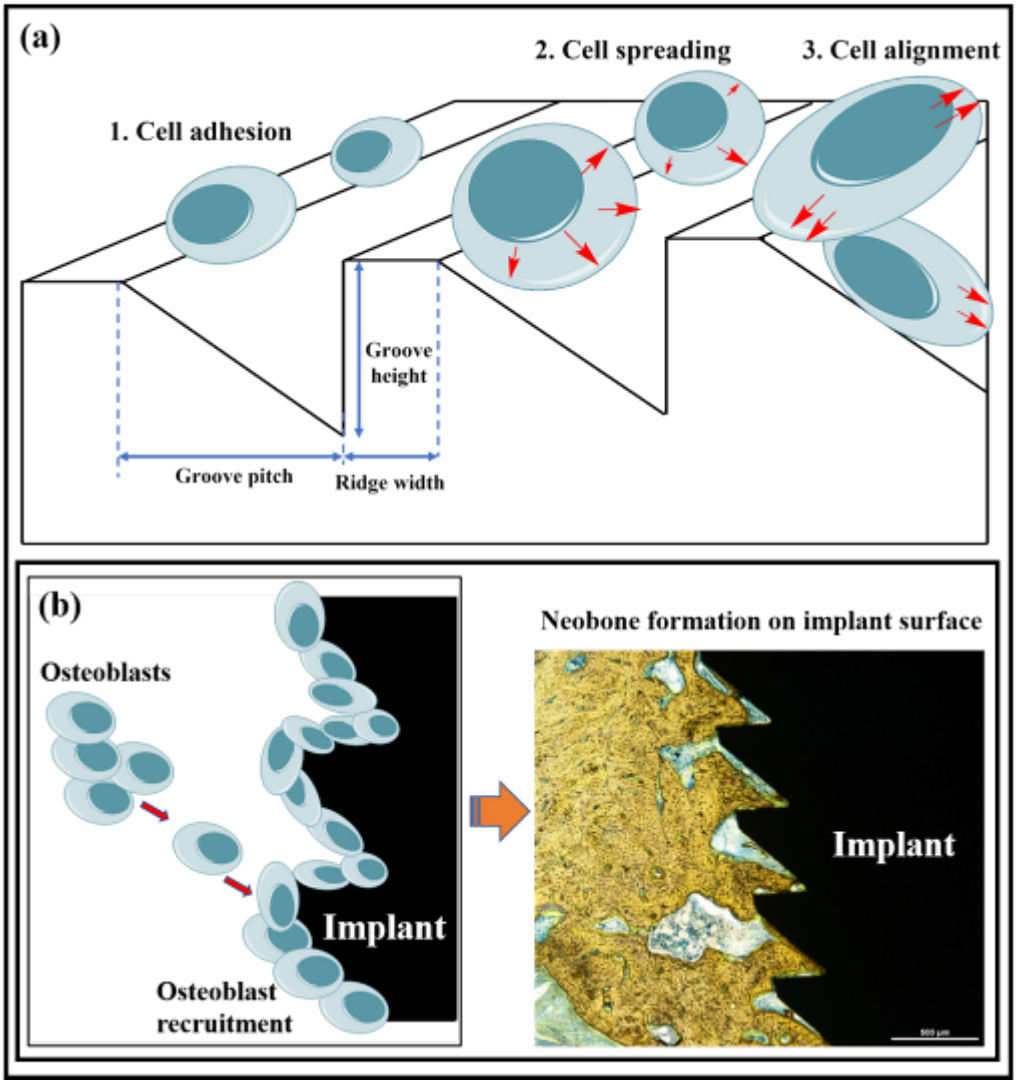

Figure 41: Cellular orientation response to microgrooves. **(a)** The contact guidance process - 1.Initially, cells adhere to the micro-grooved/grooved implant surface; 2.The adhered cells undergo spreading; 3.Cell alignment occurs, i.e., orientation along the direction of the grooves. **(b)** Contact guidance leads recruitment of more osteoblasts on the implant surface and leads to the formation of woven neobone around it.

7.3.2 Expression of osteogenic genes in the neobone formed around the implant

Micro-CT images showed better trabecular support and neobone formation around the test implant and the whole implant was continuously covered by neobone without any discontinuity. High BV/TV was observed in the case of the test implant (78.7%) compared to the control implant (67.9%), despite having no surface modification on the test implant to accelerate the process of osseointegration. The BMD of neobone formed around the test implant showed marginally lesser value than the control implant, which suggested that the process of the mineralization starts at an early stage in the case of the control implant. Yet, the expression of the RUNX2 gene is higher in case of the test implant. Also, the micro-CT tomograph of central slices has shown that the new woven bone support around the test implant is better compared to the control implant.

In this study, the expression of COL1A1, RUNX2, SPARC and VEGF genes were found to be upregulated in the case of test implant. The cells of osteoblast lineage exert various functions depending upon their differentiation stages to maintain bone formation. Previous studies have shown that, following a proliferative phase, bone cells differentiate to become more matured and begin to deposit a collagenous matrix, which is thought to influence the subsequent expression of bone proteins by osteoblastic cells.

Collagen type I (COL1A1) represents 90% of the total bone protein content. Bai et al. has reported that the COL1A1 gene expression increased while studying biomimetic osteogenic peptides in chronic inflammatory patients. The COL1A1 expression, along with other genes, indicated osteogenesis. Upregulation of COL1A1 shows that the organic phase of bone has started forming and it is dominantly forming in the case of test implant. The COL1A1 expression along with other bone markers indicated osteogenesis.

RUNX2 is a transcription factor and belongs to the *RUNX* family. RUNX2 plays an extremely important role in osteoblastic maturation, differentiation at an early stage. It also upregulate the expression of many bone matrix genes, mainly COL1A1, osteopontin (SPP1), bone sialoprotein (BSP), osteocalcin, and fibronectin. Osteonectin, encoded SPARC, a multi-functional protein with a double-action in modulating cell-cell and cell-matrix interactions and has a recognized role in functional osteoblastic differentiation of bone cells. SPARC is a highly conserved matricellular protein that modulates interactions between cells and the extracellular environment. Different studies have shown a role for SPARC in the regulation of ECM assembly, collagen formation/deposition, and growth factors signaling. High levels of SPARC, an extracellular matrix-associated glycoprotein, are associated with the development of bone and teeth by osteoblasts. SPARC is important for the collagen-binding, regulates cell growth and also has been shown to be a Ca^{2+}-binding glycoprotein that is expressed by many cell types. Delany and Hankenson studied the gene expression of SPARC in bone mineralization and proliferation; SPARC gene expression revealed the role of SPARC in the bone remodeling process. They have shown a wider pattern of activity in both mineralized and non-mineralized tissue.

SPP1 plays a role in bone regeneration and bone remodeling. In addition, it is proposed that SPP1 may be involved in the inhibition of the pathologic calcification of the bone. The observation that SPP1 and SPARC were significantly upregulated by compressive forces suggests that compressive forces regulate bone matrix synthesis and mineralization. It was earlier reported that microscale compressive loading could enhance fracture healing. SPP1 gene was found to be downregulated in both control and test implants and expressed in normal tissue. The SPP1 downregulation in newly formed bone indicates that the bone is under mineralization. Osteopontin is a non-collagenous protein in the organic phase of bone, mainly in the mineralized bone matrix. The high expression of SPP1 in the host bone is due to the mineralized bone matrix compared to the bone, surrounding the test and control implants. SPP1 has a role in bone metabolism and they are mainly seen in the mineralized tissue. A bone niche recapitulation study using the rabbit model, conducted by Minardi et al., reported the SPP1 gene expression in the mineralized bone along with other expression of other osteogenesis associated genes, for example, SPARC, COL1A1, RUNX2, etc. Foster et al. had studied the effect of osteopontin (SPP1) effect on dental mineralization and they reported that the SPP1 has been expressed in the mineralized bone in early osteoblasts, during periodontal tissue formation. Izquierdo-Barba et al. studied the effect of VEGF functionalized Ti scaffold in osteoporotic sheep. It has been observed that the VEGF scaffold promoted angiogenesis and reported an improved effect on ossification. However, surface modified implant along with the combination of micro and macro thread can effectively enhance the early onset of the osseointegration process.

7.4 Conclusions of the in vivo studies

The short-term (12 weeks) in vivo study in the rabbit model involves the quantitative and qualitative analysis of neobone regeneration and defect healing around hybrid threaded tapered test implants and a commercial control implant. Histology observations advocate that the addition of micro-threads in the newly designed dental implants clearly enhance the recruitment of osteoblasts and formation of neobone around it, even without surface modification. A higher bone integration was observed in the hybrid threaded tapered implant at 12 weeks post-implantation, with significant BV/TV values. The neobone formation and bone integration ability of the test implant was found to be superior to that of the control implant, as concluded using Micro-CT analysis, bone to implant contact and molecular gene studies. In summary, the better osseointegration of the hybrid threaded tapered implant is identified in rabbit model against the commercially available Straumann® implant.

8. OVERALL SUMMARY

8.1 The concept, rationale and objectives

The project was envisaged to explore the possibility of developing a high performing dental implant system indigenously utilizing the expertise and infrastructure available with the investigators. One aspect was to develop ceramic coatings for enhancing bioactivity as well as for the protection from wear and corrosion. These technological improvements will enhance the longevity of a dental implant. Another aspect is the performance of an indigenous implant with new design features, leading to a better healing. This involves biological experiments, *in vitro* as well as *in vivo*, to qualify the materials and implant design.

The major objectives of the project explored by the team were (i) To design a dental implant system, (ii) To fabricate the implant, (iii) To develop ceramic coating over dental implants using state-of-art coating techniques and testing their biocompatibility, (iv) To carry out the pre-clinical tests in an animal model, (v) To study the local effects or biocompatibility of surface modified dental materials using histological analysis, (vi) To study the cellular compatibility and molecular effects of dental implants via detailed bone marker analysis using RT-PCR.

8.2 Work outline

In one part of the work is the development of dual-coating concept for a dental implant. Diamond like carbon coating (DLC) over the abutments will reduce the wear during use, improve biocompatibility and resistance towards bacterial growth. DLC coating was done through Plasma Enhanced Chemical Vapour Deposition (PECVD) technique. A thin hydroxyapatite (HA) coating with a submicron uniformity over the implant lower surface will enhance the stability of the implant. Sub-micron thick conformal hydroxyapatite coating was achieved through Pulsed Laser Deposition (PLD) technique.

In the second part, a dental implant system was indigenously developed and has been tested for the local bone response by implanting in a rabbit model. Detailed study of the influence of implant design on the neobone formation was done through histology, x-ray microtomography and gene expressions in RT-PCR.

8.3 Essential results and outcomes

8.3.1 Development and evaluation of Diamond like carbon (DLC) coating

- Diamond-like Carbon coating was made on titanium and optimized, using PECVD technique in a sophisticated semi-industrial batch coating machine.
- The DLC coatings on Ti samples at optimized conditions were of high hardness, extreme smoothness and very low friction. It was found to cover the surface conformally and highly adherent to the underlying metal.

- In the *in vitro* Cyto-compatibility tests using human periodontal ligament (hPDL) cells, DLC was found non-cytotoxic and perform as a good substrate for cell adhesion and spreading.
- Bacterial adhesion and colonization on the Diamond-like carbon coating has been studied through bacterial adhesion tests. It was found that DLC coating can significantly retard bacterial adhesion.
- It was understood that DLC could be used to reduce mechanical wear of the abutment part of the implant. It is compatible to local periodontal tissues. DLC could be used to prevent bacterial biofilm formation on the abutment part in dental implant system which, in turn, will avoid post-implantation infection in the peri-prosthetic area.

8.3.2 Development and evaluation of Hydroxyapatite (HA) coating

- A semi-automated pulsed lased deposition system was used to make HA coatings. Adherent ceramic coating with excellent uniformity and homogeneous microstructure was obtained.
- The coating was found to be phase-pure hydroxyapatite (the mineral phase of bone) which is a biocompatible and bioactive material.
- The coatings were thin and free of cracks. Therefore, the peel-off problems will be less compared to commercial plasma-spray coated HA.
- The interaction of human osteosarcoma cells on HA coating was investigated through *in vitro* cell culture. The cells on HA coated surfaces showed adhesion and proliferation, in SEM and Confocal Microcopy. The HA coating enhances the bioactivity of Ti surface.
- The screw part of the implant system was coated with hydroxyapatite through semi-automated PLD process. The coating was smooth to micron level and covered the contours of the threads.
- As the HA coating supported the growth and proliferation of cells, it would be a good candidate to promote osseointegration of the screw part of titanium implant.

8.3.3 Additional explorations

(i) <u>Alternative materials for implant coating</u>

- Tricalcium phosphate (α-TCP) has been identified as an alternative material for implant coating. Owing to the *in vivo* reactivity, this will promote osseointegration of the screw part of titanium implant.
- Indigenously synthesized α-TCP was used as the target material for coating over titanium surface using PLD technique.
- Correct phase of the material was obtained in the coating.

(ii) New process for implant surface modification

- A simple and effective technique of attaching calcium ions onto titanium surface through hydrothermal method was developed. This process will provide osseointegration, and avoid a separate physical coating and the related peel off problems.
- The process involves initial etching of Ti surface and hydrothermal modification using Ca(OH)2 solution at temperature 200°C and pressure 200 bars for 5h.
- The surface was found to be covered with a nano-level coating. XPS study revealed that the coated material consist of CaO and CaTiO3.
- The biomineralization behavior of the modified surface of titanium was evaluated in simulated body fluid concentrate. It was found that apatitic calcium phosphate deposition occurs on the surface. Characterization showed phase-pure apatite formation. This indicates the capacity of the modified surface for osseointegration.
- The cytocompatibility of the coating was analysed in vitro through 'Direct contact test' and MTT assay preliminary test using L929 mouse fibroblast cells. The coating passed both the tests.
- The adhesion and proliferation of mouse fibroblast cells on the coating were analysed through *in vitro* cell culture. It was found that the cells attach and grow over the surface.
- These results indicated that the surface modification via hydrothermal treatment created calcium rich nanolayer formation on titanium which will potentially promote bone apposition in the process of *in vivo* implantation.

8.3.4 Design development of indigenous implant system

- A complete dental implant system, with screw and abutment, has been developed by the design team, based on the first principles of dental implants.
- The implant screw part is shaped into the conical / tapered screw of with 5.0 mm diameter at the upper threaded end and 3 mm at the lower threaded end, terminating with a dome of 2.5 mm radius. This is to reduce the resistance in bone while implantation.
- Micro V-threads are given on the collar region and the apical or tapered portion was provided with buttress threads having with 45° alignment.
- The implant contains a straight healing chamber also. The primary purpose of the healing chamber is to harbour bone chips and blood during the implant insertion.
- The abutment part has a modified fitting for better stability.

8.3.5 Bone implantation studies in animal model

(i) The implantation process

- The animal experiments were done in a facility approved for animal care and having a dedicated operation theatre. The work was done as per the International Standards, keeping all ethical practices and following regulatory stipulations.
- The implantation procedures were managed by expert animal surgeon, dental implant consultant and histopathologist.
- New Zealand White crabbit breed was selected for the study. The maintenance and care of animals were arranged as per accepted International Standards.
- The new dental implant design made by the investigators' team has been fabricated for the test. For comparison, a commercial brand was used.
- The newly designed implant (the test samples) and the commercial brand implant (the control samples) were inserted in the femoral condylar area of New Zealand white rabbits, as per standard procedure. The implantation was done on 10 animals with the test implant on the left limb and control implant on the right limb.
- After the stipulated time period of 12 weeks, each implant along with the surrounding tissues, was removed and preserved for further evaluation.

(ii) Local effects after implantation

- The explanted sites were subjected to gross view. The implants showed good apposition to bone and were stable after the implantation period. In histopathology slides, the new bone in the defect area was in close contact with the implant surface. The test implant was having more bone contact.
- The Micro-CT images showed better trabecular support and neobone formation around the test implant compared to the control implant. In the case of test implant, it was covered by neobone without any discontinuity.
- In histological observation, the sections of the implanted bone under the microscope did not show any evidences for necrosis, inflammation or degeneration at the implant-bone interface. No intervening soft tissue nor any fluid collection or breaks was observed between the implant and bone.
- In the sections of the test site, new woven bone and lamellar bone were observed following the thread morphology. The control implant revealed multiple areas of implant surface not covered with neobone.
- Multiple foci of neobone formation with rosettes of osteoblasts were noted at the interface of both control and test implants. Mature new woven bone and lamellar bone were observed with well-developed 'Haversian system' or 'osteons' along the test implant thread geometry.

(iii) Molecular level events in healing

- Gene expression of the test and control samples was tested by RT-PCR method. The expression of osteogenic genes COL1A1, RUNX2 and SPARC were up-regulated in the new implant, indicating that the bone is in the mineralization phase.

8.4 Salient achievements

As the final note after summing up the course of the project, it could be stated that all the objectives are met. There are a few notable technological outcomes as given below.

- ✓ Demonstration and optimization of coating of Diamond like Carbon (DLC) through PECVD, was done. This is a promising technology to protect the abutment part of the dental implant which undergo heavy cyclic loading of mastication.
- ✓ Demonstration of making a thin and robust coating of hydroxyapatite (HA) through PLD, was done. This coating is superior to the currently available plasma spray coating of HA, related to microstructure and robustness.
- ✓ A new surface modification technique has been developed to make titanium metal bioactive. This is done by creating a calcium rich nanolayer on titanium via hydrothermal treatment. If commercially viable, this will be an affordable method for creating bone compatible titanium implant surface.
- ✓ A dental implant system has been designed and developed indigenously. This has certain useful features like tapered shape, dual threading and healing chamber. The new implant has been fabricated considering the commercial viability.
- ✓ The pre-clinical tests of the newly designed implant have been done in Rabbit model. The local effects of the implant were studied using histological analysis. Also the cellular and molecular effects were investigated. The result showed that the implant was stable and tissue compatible.
- ✓ The new implant design promoted neobone growth at the implant site and good bone apposition to implant was noted.
- ✓ The success in this pre-clinical experiment declares that the new implant designed in this project has qualified the Technology Readiness level of 5 (TRL5). The next is the human clinical trial stage (TRL6), to be initiated after the technology transfer.
- ✓ Discussions are ongoing with the industry so as to transfer the technology.
- ✓ The documents and reports generated related to the implant design and the various tests and analyses, will contribute to the regulatory documentation for test manufacturing license and marketing license, once the technology is transferred.